NASA/TM-2001-211227
ARL-TR-2568

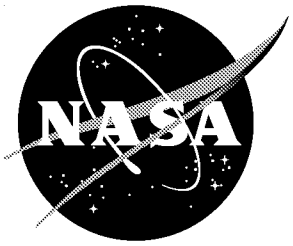

Analysis of Ninety Degree Flexure Tests for Characterization of Composite Transverse Tensile Strength

T. Kevin O'Brien
U.S. Army Research Laboratory
Vehicle Technology Directorate
Langley Research Center, Hampton,Virginia

Ronald Krueger
ICASE
NASA Langley Research Center
Hampton, Virginia

October 2001

The NASA STI Program Office ... in Profile

Since its founding, NASA has been dedicated to the advancement of aeronautics and space science. The NASA Scientific and Technical Information (STI) Program Office plays a key part in helping NASA maintain this important role.

The NASA STI Program Office is operated by Langley Research Center, the lead center for NASA's scientific and technical information. The NASA STI Program Office provides access to the NASA STI Database, the largest collection of aeronautical and space science STI in the world. The Program Office is also NASA's institutional mechanism for disseminating the results of its research and development activities. These results are published by NASA in the NASA STI Report Series, which includes the following report types:

- TECHNICAL PUBLICATION. Reports of completed research or a major significant phase of research that present the results of NASA programs and include extensive data or theoretical analysis. Includes compilations of significant scientific and technical data and information deemed to be of continuing reference value. NASA counterpart of peer-reviewed formal professional papers, but having less stringent limitations on manuscript length and extent of graphic presentations.

- TECHNICAL MEMORANDUM. Scientific and technical findings that are preliminary or of specialized interest, e.g., quick release reports, working papers, and bibliographies that contain minimal annotation. Does not contain extensive analysis.

- CONTRACTOR REPORT. Scientific and technical findings by NASA-sponsored contractors and grantees.

- CONFERENCE PUBLICATION. Collected papers from scientific and technical conferences, symposia, seminars, or other meetings sponsored or co-sponsored by NASA.

- SPECIAL PUBLICATION. Scientific, technical, or historical information from NASA programs, projects, and missions, often concerned with subjects having substantial public interest.

- TECHNICAL TRANSLATION. English-language translations of foreign scientific and technical material pertinent to NASA's mission.

Specialized services that complement the STI Program Office's diverse offerings include creating custom thesauri, building customized databases, organizing and publishing research results ... even providing videos.

For more information about the NASA STI Program Office, see the following:

- Access the NASA STI Program Home Page at *http://www.sti.nasa.gov*

- E-mail your question via the Internet to help@sti.nasa.gov

- Fax your question to the NASA STI Help Desk at (301) 621-0134

- Phone the NASA STI Help Desk at (301) 621-0390

- Write to:
  NASA STI Help Desk
  NASA Center for AeroSpace Information
  7121 Standard Drive
  Hanover, MD 21076-1320

NASA/TM-2001-211227
ARL-TR-2568

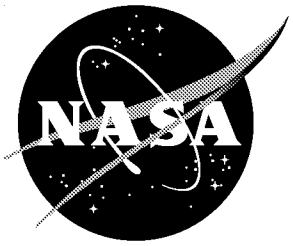

Analysis of Ninety Degree Flexure Tests for Characterization of Composite Transverse Tensile Strength

T. Kevin O'Brien
U.S. Army Research Laboratory
Vehicle Technology Directorate
Langley Research Center, Hampton,Virginia

Ronald Krueger
ICASE
NASA Langley Research Center
Hampton, Virginia

National Aeronautics and
Space Administration

Langley Research Center
Hampton, Virginia 23681-2199

October 2001

The use of trademarks or names of manufacturers in the report is for accurate reporting and does not constitute an official endorsement, either expressed or implied, of such products or manufacturers by the National Aeronautics and Space Administration or the U.S. Army.

Available from:

NASA Center for AeroSpace Information (CASI)
7121 Standard Drive
Hanover, MD 21076-1320
(301) 621-0390

National Technical Information Service (NTIS)
5285 Port Royal Road
Springfield, VA 22161-2171
(703) 605-6000

Analysis of Ninety Degree Flexure Tests for Characterization of Composite Transverse Tensile Strength

T. Kevin O'Brien [1] and Ronald Krueger [2]

[1] *U.S. Army Research Laboratory, Vehicle Technology Directorate*
[2] *ICASE*
NASA Langley Research Center, Hampton, Virginia, U.S.A.

SUMMARY: Finite element (FE) analysis was performed on 3-point and 4-point bending test configurations of ninety degree oriented glass-epoxy and graphite-epoxy composite beams to identify deviations from beam theory predictions. Both linear and geometric non-linear analyses were performed using the ABAQUS® finite element code. The 3-point and 4-point bending specimens were first modeled with two-dimensional elements. Three-dimensional finite element models were then performed for selected 4-point bending configurations to study the stress distribution across the width of the specimens and compare the results to the stresses computed from two-dimensional plane-strain and plane-stress analyses and the stresses from beam theory. Stresses for all configurations were analyzed at load levels corresponding to the measured transverse tensile strength of the materials.

For 3-point bend test configurations, both the linear and geometric non-linear 2D plane-strain and plane-stress analyses yielded similar results. The maximum tensile stresses under the center load nose calculated from the FE analysis were slightly lower than stresses predicted by beam theory. The difference (maximum of 4%) was greatest for the shortest span analyzed.

For 4-point bend test configurations, both the plane-stress and plane-strain 2D linear analysis results agreed closely with beam theory except right below the load points. However, 2D geometric non-linear analyses deviated slightly from beam theory throughout the inner span as well as below the load points. Plane-stress results deviated from beam theory more than plane-strain results. The maximum tensile stresses between the inner span load points were slightly greater than the beam theory result. This difference was greatest (maximum of 4%) for configurations with the shortest spans between inner and outer load points. A contact analysis was also performed in order to investigate the influence of modeling the roller versus modeling the support as a simple boundary condition at one nodal point. A configuration with the shortest span between inner and outer load points was modeled for the 24-ply and 36-ply IM7/8552 layups and the 24-ply S2/8552 layup. Generally, for all configurations investigated, the discrepancy between the FE and beam theory results became smaller (max. 2%) when the rollers were

modeled in conjunction with contact analysis. Hence, the beam theory yields a reasonably accurate value for the maximum tensile stress in bending compared to 2D FE analysis.

The 3D linear FE analysis of the 4-point configurations agreed closely with beam theory, except right below the load points. The 3D linear FE results at the specimen edge agreed with 2D plane-stress results, and the 3D linear FE results in the center of the specimen agreed with 2D plane-strain results. The 3D geometric non-linear analyses deviated slightly from beam theory throughout the inner span as well as under load points. The 3D geometric non-linear FE results at the specimen edge agreed with the 2D plane-stress results. For the 12.7 mm (0.50 in.) wide IM7/8552 specimens, the 3D geometric non-linear FE results in the center of the specimen agreed with 2D plane-strain results. However, for the 6.35 mm (0.25 in.) wide S2/8552 specimens, the 3D geometric non-linear FE results in the center were less than 2D plane-strain results, indicating that these specimens were not wide enough to achieve full constraint.

The utility of the FE results is primarily for guidance in the choice of beam thickness, width, and configuration. For the 3-point bend configuration, longer spans are preferred to minimize the error in beam theory data reduction. Similarly, for the 4-point bend configurations, a longer span between the inner and outer load noses, at least equal to the span between the inner load noses, results in less error compared to beam theory. In addition, these FE results indicate that the span between the inner load noses should not be too long to avoid obtaining a non-uniform maximum stress between the inner load noses. Finally, the 3D analysis indicates that specimens should be sufficiently wide to achieve a fully constrained state of plane-strain at the center of the specimen width.

KEYWORDS: transverse tensile strength, matrix cracking, finite element analysis, glass epoxy, graphite epoxy, bending tests

INTRODUCTION

Matrix ply cracking is a common initial damage mechanism in fiber reinforced composites. Matrix ply cracking alone is seldom catastrophic for laminates subjected to membrane loading. However, for composite structures that undergo bending, or other out-of-plane loading, the formation of matrix cracks may lead to immediate catastrophic delamination formation and growth [1,2]. Hence, accurate characterization of the transverse tensile strength of composite materials is needed to accurately predict matrix ply cracking in these structures.

Previously, 90 degree unidirectional glass-epoxy laminates [3] and carbon-epoxy laminates [4] were tested in three and four point bending to characterize composite transverse tensile strength. The influence of edge flaws due to machining, and surface flaws due to manufacture and handling, were assessed by testing specimens in their as-manufactured and machined condition. In addition, specimens with polished edges, and/or bottom failure surfaces, were tested. Subsequent 3-point and 4-point bend tests of glass-epoxy lamina and carbon-epoxy lamina [5] were also performed under cyclic

loading. In each of these studies, the maximum tensile stress at failure under monotonic and cyclic loading was determined using beam theory expressions.

The goal of this investigation was to study under which conditions simple beam theory yielded sufficiently accurate results when used to calculate the stresses in the 3-point and 4-point bending specimens. For the entire investigation, the ABAQUS® finite element software was used. For comparison, both linear and geometric nonlinear analysis procedures were used. The three-point and four-point bending specimens were first modeled entirely with two-dimensional elements. Then, three-dimensional finite element models were used to study the stress distribution across the width of the specimens and compare the results to the stresses computed from two-dimensional plane-strain and plane-stress analyses and the stresses from simple beam theory.

Materials

FE analyses were performed on two materials, S2/8552 glass-epoxy [3,5] and IM7/8552 carbon-epoxy [4,5]. Material properties used in the analysis are given in Table 1. The S2/8552 specimens were cut from a 24-ply panel. The average panel thickness was 5.56 mm, corresponding to an average ply thickness of 0.231 mm. The IM7/8552 specimens were cut from both 24-ply and 36-ply panels. The average panel thickness was 3.29 mm for the 24-ply panel and 4.94 mm for the 36-ply panel, corresponding to an average ply thickness of 0.137 mm.

Specimen Configurations

Three-point bending tests were evaluated in three configurations (A, B, and C) corresponding to span lengths of 25.4, 50.8, and 76.2 mm (figure 1(a)). Four point bending tests were evaluated using the four configurations (A1, A2, B2, B3) shown in figure 1(b).

Beam Theory

For the three point bending configurations shown in figure 1(a), with span length, s, and width, b, the tensile bending stress distribution at the bottom of the beam is shown in figure2a. Specimen strengths were determined in references 3&4 from the beam theory expression for the maximum tension stress, σ_{max}, under the center load nose using the maximum load at failure, P_c, and the average specimen thickness, t_{avg},

$$\sigma_{max} = \frac{3P_c s}{2bt_{avg}^2} \quad . \tag{1}$$

For the four point bending tests shown in figure 1(b), with outer span, s, inner span, s-ℓ, and width, b, the tensile bending stress distribution at the bottom of the beam is shown in figure 2b. Specimen strengths were determined in references 3&4 from the beam theory

expression for the maximum uniform tension stress, σ_{max}, between the inner load points using the maximum load at failure, P_c, and the average specimen thickness, t_{avg},

$$\sigma_{max} = \frac{3P_c\ell}{2bt_{avg}^2} \tag{2}$$

Finite Element (FE) Analysis Formulation

Two typical two-dimensional finite element models of the specimens, boundary conditions and loads applied in the simulations are shown in Figure 3. A typical three-dimensional finite element model of the specimens used in the simulations is shown in Figure 4. For both the 2D and 3D analyses, the ABAQUS® input file was generated automatically using a FORTRAN routine (see Appendix 1). This user-written routine required only the input of the geometrical data, the material property data given in Table I, and the mesh parameters shown in Figure 3. The use of this routine allowed the quick generation of a large number of models for the different specimen configurations and simplified the otherwise tedious mesh generation and refinement.

The two-dimensional specimen cross sections were modeled using eight-noded quadrilateral plane-strain (CPE8R) or plane-stress (CRS8R) elements using quadratic shape functions and a reduced (2x2) integration scheme. These elements were selected to avoid shear locking in bending, which is common in first-order, fully integrated elements, such as CPE4 and CPS4 [6]. The numerical formulation of first order elements gives rise to shear strains that do not really exist. Therefore, these elements are too stiff in bending, and many elements over the thickness are required to obtain acceptable results. Elements where a lower-order, reduced integration are used to form the element stiffness, such as the CPE8R and CPS8R elements used in this study, usually require fewer elements through the thickness, provide more accurate results in bending, and yield reduced running times. Loads were prescribed at single nodal points in the models. However, for configuration B2 that exhibited the greatest deviation from beam theory, rollers were also included in the model at the outside load points (see Appendix 2).

For the 3D analyses, specimens were modeled with ABAQUS® solid, twenty-noded, C3D20R hexahedral elements using quadratic shape functions and a reduced (2x2x3) integration scheme. The C3D20R element utilizes reduced integration to form the element stiffness, and hence, provides accurate results in bending which yield reduced running times compared to other 3D elements [6,7].

Computation of Stresses

Averaged stresses at nodes were computed along the bottom (tension) surface of the beam specimens where the highest tensile stresses occur. The results were extracted for additional post-processing directly from the ABAQUS® binary result file using a user written FORTRAN routine (See Appendix 1) [6,7].

Two Dimensional FE Analysis Results

Three Point Bending

Figure 5 shows the finite element mesh for the S2/8552 glass epoxy material, 3-point bend configuration A (figure1a). The mesh is shown in the deformed position at the failure load with the stress contours superimposed illustrating the compression stress near the point of load application at the top of the beam and the high tensile stresses at the bottom of the beam under the center load nose. Tension stress results at the bottom of the beam will be quantified in later figures. Similar meshes were generated for the other 3-point bend configurations in figure 1a using the technique described earlier.

The open symbols in figure 6 show the stresses calculated from the 2D, plane-strain, linear finite element analysis, σ_{FE}, normalized by the maximum tension stress calculated from the beam theory, σ_{BT} (σ_{max} in equation 1). For comparison, the normalized stress distribution from beam theory is superimposed on the finite element results. This comparison indicates that the peak tensile stress calculated from the finite element analysis is slightly (4%) less than the beam theory prediction. Similar results were obtained for the 2D plane-stress linear finite element analysis, as well as the 2D geometric non-linear plane-strain and plane-stress FE analyses. In order to establish the accuracy of this comparison, the 2D geometric non-linear analysis was also performed using a refined mesh as shown in figure 7. This analysis yielded more stress results in the critical area under the load nose. However, this refined mesh yielded essentially no change in the maximum stress calculated directly under the load nose, which was also less than the beam theory (figure 8).

Figure 9 summarizes the peak stress comparisons for the 24-ply S2/8552 glass-epoxy 3-point bend configurations in terms of percent $\Delta\sigma$, where

$$\Delta\sigma = \frac{\sigma_{BT} - \sigma_{FE}}{\sigma_{BT}} \text{x}100 \tag{3}$$

As shown in figure 9, the greatest difference between all the 2D FE analyses and the beam theory was about 4% for the shortest span, configuration A. The longer span configurations had difference between 1 % and 2%.

Figure 10 summarizes the peak stress comparisons for the 24-ply IM7/8552 carbon–epoxy 3-point bend configurations. The greatest difference between all the 2D FE analyses and the beam theory was about 2% for the shortest span, configuration A. The longer span configurations had differences of 1 % or less. Figure 11 summarizes the peak stress comparisons for the 36-ply IM7/8552 carbon–epoxy 3-point bend configurations. The greatest difference between all the 2D FE analyses and the beam theory was about 3% for the shortest span, configuration A. The longer span configurations had difference between 1 % and 2%.

The results from figures 10-11 indicate that the beam theory results become less accurate for thicker beams of a given span, and for shorter spans of the same beam thickness. This is the same trend expected for the significance of transverse shearing deformation in 3-point bending of beams. This shearing deformation is not reflected in the beam theory equations 1 and 2.

Four Point Bending

Figure 12 shows the finite element mesh for the S2/8552 glass-epoxy material, 4-point bend configuration A1 (figure1b). The mesh is shown in the deformed position at the failure load with the stress contours superimposed illustrating the compression stress between the two inner load noses at the top of the beam and the high tensile stresses at the bottom of the beam under the inner load noses. Tension stress results at the bottom of the beam will be quantified in later figures. Similar meshes were generated for the other 4-point bend configurations in figure 1b using the technique described earlier.

The open symbols in figure 13 show the stresses calculated from the 2D plane-strain, linear finite element analysis, σ_{FE}, normalized by the maximum tension stress calculated from the beam theory, σ_{BT} (σ_{max} in equation 2). For comparison, the normalized stress distribution from beam theory is superimposed on the finite element results. This comparison indicates that the peak tensile stress calculated from the finite element analysis is slightly less than the beam theory prediction just below the load nose as observed in the 3-point bend case. However, the 4-point bend FE results become slightly greater than the beam theory stress just inside the load nose before assuming the beam theory result in the majority of the span between the inner load noses. Similar results were obtained for the 2D plane-stress, linear finite element analysis. The 2D plane-strain geometric non-linear FE analysis yielded a similar FE stress distribution, except the plateau in the majority of the span between the inner load noses was larger (1.5%) than the beam theory result (figure 14). The 2D plane-stress, geometric non-linear FE analysis, yielded a similar FE stress distribution, but with an even greater discrepancy (2.5%) from the beam theory between the two center load noses (figure 15). In order to establish the accuracy of this comparison, the 2D geometric non-linear analysis was also performed using a refined mesh as shown in figure 16. This yielded more stress results between the inner load noses, but there was essential no change in the plateau of the distribution between the inner load noses (figure 17). Figures 18 a-d compare the 2D geometric non-linear plane-strain and plane-stress results in terms of percent $\Delta\sigma$ (equation 3) between the inner load noses for the four S2/8552 glass-epoxy 4-point bend configurations (figure1b). For all four configurations, the plane-stress results differ from the beam theory predictions by 0.5 to 1.5% more than the plane-strain results.

The 2D plane-stress geometric non-linear FE results in terms of percent $\Delta\sigma$ (equation 3) between the inner load noses are summarized for all four S2/8552 glass epoxy 4-point bend configurations in figure 19. For the plateau in the majority of the span between the inner load noses, the greatest discrepancy between the FE and beam theory results occurs for configurations B2 (4%) and A1 (2.5%). These two configurations have the shortest

span between the inner and outer load noses (12.7 mm). Figure 19 also illustrates the non-uniform stress distribution between the inner load noses for the two configurations, B2 and B3, with the greatest inner span, s-ℓ = 50.8 mm. These same trends were noted for the 24-ply (figure 20) and 36-ply (figure 21) IM7/8552 carbon-epoxy, 4-point bend configurations. The thinner 24-ply laminate had slightly lower discrepancies (only 3% for configuration B2, for example) than the thicker 36-ply laminate of the same material. However, the non-uniform stress distribution between the inner load noses was more pronounced in the thinner laminates.

Contact Analysis

A contact analysis was performed in order to investigate the influence of modeling the roller versus modeling the support as a simple boundary condition at one nodal point (see appendix 2). It was expected that accounting for the roller would change the contact location and result in a shorter span, s, of the specimen and thus result in a different stress distribution along the bottom surface of the specimen. The roller support was modeled and corresponding contact analysis was performed for specimen configuration B2, only, because discrepancy in stresses between the finite element and the beam theory results were most pronounced for this configuration as shown in Figures 19-21. The B2 configuration was modeled for the 24-ply and 36-ply IM7/8552 layups and the 24-ply S2/8552 layup. As shown in the appendix, for all configurations investigated the discrepancy between the FE and beam theory results became smaller (max. 3%) when the rollers were modeled in conjunction with contact analysis instead of simple supported boundary conditions. Hence, the beam theory yields a reasonably accurate value for the maximum tensile stress in bending compared to 2D FE analysis.

Three Dimensional FE Analysis results

The S2/8552 glass-epoxy material, 4-point bend configuration B2 (figure1b) was chosen for the 3D analysis since it exhibited the greatest deviation from beam theory in the 2D non-linear analysis. Figure 22 shows the finite element mesh for a 6.35mm wide S2/8552 glass-epoxy, 4-point bend configuration B2. The mesh is shown in the deformed position at the failure load. The 3D model had the same in-plane mesh refinement as the 2D analyses, but with ten elements across the specimen width.

Figure 23 shows the 3D geometric non-linear FE stress results in terms of percent $\Delta\sigma$ (equation3) between the inner load noses and across the specimen width. Near the load noses, the stresses peak near the center of the specimen width. However, between the load noses the stress peaks near the edges of the specimen. Ideally, the stresses calculated near the specimen edges should be in good agreement with the 2D plane-stress results and the stresses calculated near the center of the specimen should be in good agreement with the 2D plane-strain results. Figure 24a compares the 3D stresses at the specimen edge to the 2D plane-stress results for both the linear and geometric non-linear cases. Good agreement was found in both cases, with only the non-linear case showing the significant deviation from the beam theory result between the inner load noses. Figure 24b compares the 3D stresses at the center of the specimen width to the 2D plane-strain

results for both the linear and geometric non-linear cases. Good agreement was found for the linear case, with no significant deviation from the beam theory result between the inner load noses. However, the 3D non-linear case indicated a greater deviation from the beam theory result between the inner load noses (4%) than did the 2D plane-strain result (3%). This indicated that these beams were not quite wide enough to achieve a fully constrained (plane-strain) condition at the specimen center.

To investigate the influence of specimen width further, a 3D analysis was also performed for a 12.7mm wide, 24-ply, IM7/8552 carbon-epoxy, 4-point bend configuration A1 (figure1b). This configuration was used in reference 5 to characterize transverse tension fatigue life. Figure 25 shows the finite element mesh for the 24-ply, IM7/8552 graphite-epoxy material, 4-point bend configuration A1. The mesh is shown in the deformed position at the failure load. The 3D model had the same in-plane mesh refinement as the 2D analyses, but with ten elements across the specimen width.

Figure 26 shows the 3D geometric non-linear FE stress results in terms of percent $\Delta\sigma$ (equation 3) between the inner load noses and across the specimen width. Figure 27a compares the 3D stresses at the specimen edge to the 2D plane-stress results for both the linear and geometric non-linear cases. Good agreement was found in both cases, with only the non-linear case showing a slight deviation (1.5 %) from the beam theory result between the inner load noses. Figure 27b compares the 3D stresses at the center of the specimen width to the 2D plane-strain results for both the linear and geometric non-linear cases. Good agreement was found for the linear case, with no significant deviation from the beam theory result between the inner load noses. Furthermore, for this 12.7 mm wide specimen, there was also good agreement between the 2D non-linear plane-strain solution and the 3D non-linear solution at the center of the specimen width, indicating that a fully constrained (plane-strain) condition had been achieved at the specimen center. Both the 2D and 3D non-linear analyses results indicated a slight (1.5%) deviation from the beam theory at the specimen center.

Analysis of Results

Figures 28-30 compare the 2D stress analysis results for 3-point bend configurations A, B, and C for the S2/8552, 24-ply IM7/8552, and 36-ply IM7/8552 materials, respectively, to the histogram of failure locations measured for these materials [4]. The histograms show the location and frequency of failures for the number of replicates tested of a given configuration. These figures indicate that most failures occur near the center of the span, but not always directly below the central load nose where the tensile stress is a maximum (figure 2a). As noted in references 3-5, all failures do not occur directly below the load nose because the failure is sensitive to the presence of flaws in the specimen microstructure. Both the beam theory and the finite element analysis assume that the material is uniform and homogeneous throughout. Hence, it would be meaningless to reduce the data based on the FE stress at a given span location relative to the center load nose because the failure is due to the local stresses associated with micro-structural flaws. Rather, in order to characterize the strength and the associated volume dependence, data

are fit to either a normal or Weibull distribution ranked according to the calculated maximum stress at failure from the beam theory [4,5].

Figures 31 a-d compare the 2D stress analysis results for 4-point bend configurations A1, A2, B2, and B3, respectively, for the S2/8552 glass epoxy material to the histogram of failure locations measured for these materials [3,4]. These figures indicate that most failures occur near the center of the span, between the inner two load noses where the tensile stress is a maximum (figure 2b). The remaining failures occur below the inner load noses as was observed in the 3-point bend specimens.

Figures 32 a-c compare the 2D stress analysis results for 4-point bend configurations A1, A2, and B2, respectively, for the 24-ply IM7/8552 carbon-epoxy material to the histogram of failure locations measured for these materials [4]. Figures 33 a-d compare the 2D stress analysis results for 4-point bend configurations A1, A2, B2, and B3, respectively, for the 36-ply IM7/8552 carbon-epoxy material to the histogram of failure locations measured for these materials [4]. Unlike the glass-epoxy material, a greater percentage of failures occur below the inner load noses for all the configurations. In reference 4, this was attributed to the large variability in specimen thickness observed in the graphite material, which is not accounted for in either the beam theory or FE analysis, but leads to a biased loading towards one, or the other, inner load noses in the experiments.

The utility of the FE results is primarily for guidance in the choice of beam thickness, width, and configuration. For the 3-point bend configuration, longer spans are preferred to minimize the error in beam theory data reduction. Similarly, for the 4-point bend configurations, a longer span between the inner and outer load noses, at least equal to the span between the inner load noses, results in less error compared to beam theory. In addition, these FE results indicate that the span between the inner load noses should not be too long to avoid obtaining a non-uniform maximum stress between the inner load noses. Finally, the 3D analysis indicates that specimens should be sufficiently wide to achieve a fully constrained state of plane-strain at the center of the specimen width.

Conclusions

For 3-point bend test configurations, both the linear and geometric non-linear 2D plane-strain and plane-stress analyses yielded similar results. The maximum tensile stresses under the center load nose calculated from the finite element (FE) analysis were slightly lower than stresses predicted by beam theory. The difference (maximum of 4%) was greatest for the shortest span analyzed.

For 4-point bend test configurations, both the plane-stress and plane-strain 2D linear analysis results agreed closely with beam theory except right below the load points. However, 2D geometric non-linear analyses deviated slightly from beam theory throughout the inner span as well as below the load points. Plane-stress results deviated from beam theory more than plane-strain results. The maximum tensile stresses between the inner span load points were slightly greater than the beam theory result. This

difference was greatest (maximum of 4%) for configurations with the shortest spans between inner and outer load points. A contact analysis was also performed in order to investigate the influence of modeling the roller versus modeling the support as a simple boundary condition at one nodal point. The B2 configuration was modeled for the 24-ply and 36-ply IM7/8552 layups and the 24-ply S2/8552 layup. Generally, for all configurations investigated, the discrepancy between the FE and beam theory results became smaller (max. 2%) when the rollers were modeled in conjunction with contact analysis. Hence, the beam theory yields a reasonably accurate value for the maximum tensile stress in bending compared to 2D FE analysis.

The 3D linear FE analysis of the 4-point configurations agreed closely with beam theory, except right below the load points. The 3D linear FE results at the specimen edge agreed with 2D plane-stress results, and the 3D linear FE results in the center of the specimen agreed with 2D plane-strain results. The 3D geometric non-linear analyses deviated slightly from beam theory throughout the inner span as well as under load points. The 3D geometric non-linear FE results at the specimen edge agreed with the 2D plane-stress results. For the 12.7 mm (0.50 in.) wide IM7/8552 specimens, the 3D geometric non-linear FE results in the center of the specimen agreed with 2D plane-strain results. However, for the 6.35 mm (0.25 in.) wide S2/8552 specimens, the 3D geometric non-linear FE results in the center were less than 2D plane-strain results, indicating that these specimens were not wide enough to achieve full constraint.

The utility of the FE results is primarily for guidance in the choice of beam thickness, width, and configuration. For the 3-point bend configuration, longer spans are preferred to minimize the error in beam theory data reduction. Similarly, for the 4-point bend configurations, a longer span between the inner and outer load noses, at least equal to the span between the inner load noses, results in less error compared to beam theory. In addition, these FE results indicate that the span between the inner load noses should not be too long to avoid obtaining a non-uniform maximum stress between the inner load noses. Finally, the 3D analysis indicates that specimens should be sufficiently wide to achieve a fully constrained state of plane-strain at the center of the specimen width.

References

1) Minguet, P.J, and O'Brien, T.K., "Analysis of Test Methods for Characterizing Skin/Stringer Debonding Failures in Reinforced Composite Panels", *Composite Materials: Testing and Design, Twelfth Volume, ASTM STP 1274*, August, 1996, p.105-124.

2) O'Brien, T.K., and Sen, J.K., "Tension-Torsion Behavior of Glass Epoxy Flexbeam Laminates", *ASTM Journal of Composites Technology and Research, JCTRER*, Vol. 20, No.4, October, 1998, pp. 221-226.

3) O'Brien, T.K., Chawan, A.D., and DeMarco, K.,: Influence of Specimen Preparation and Specimen Size on the Transverse Tensile Strength and Scatter of Glass Epoxy Laminates, Proceedings of the Twelfth International Conference on Composite Materials (ICCM XII), Paris, France, July, 1999, paper 976, ISBN 2–9514526–2–4,

4) O'Brien, T. K., Chawan, A.D., DeMarco, K., and Paris, I.L,: Influence of Specimen Preparation and Specimen Size on Composite Transverse Tensile Strength and Scatter, NASA TM-2001-211030, ARL-TR-2540, July, 2001.

5) O'Brien, T.K., Chawan, A.D., Krueger, R., and Paris, I.S.,: Transverse Tension Fatigue Life Characterization through Flexure Testing of Composite Materials, NASA TM-2001-211035, ARL TR 2544, July, 2001 (Accepted for publication in the *International Journal of Fatigue*).

6) ABAQUS/Standard, "User's Manual, Volume II," Version 5.6, 1996.

7) Krueger, R., and O'Brien, T.K., "A Shell/3D Modeling Technique for the analysis of delaminated composite laminates," *Composites Part A: applied science and manufacturing*, vol. 32, January, 2001, pp. 25-44.

Acknowledgements

This study was performed as part of Cooperative Research and Development Agreements (CRDA) between Bell Helicopter Company and the Boeing Company, Philadelphia, and the U.S. Army Research Laboratory, Vehicle Technology Directorate, located at NASA Langley Research Center.

Appendix 1

A general overview of the analysis procedure is given in Figure A1. The ABAQUS® input file was generated automatically using a user written FORTRAN routine (genbeam.f in figure A1), which, in addition to the material data given in Table I, only required the input of the loading, the geometrical data and mesh parameters as shown in Figures 3 and 4. The use of this routine (flow chart shown in Figure A2) allowed the quick generation of a large number of models for the different specimens and simplified the otherwise tedious mesh refinement and convergence studies.

The stresses along the bottom side/surface of the beam specimens were of prime interest as this is the location where the highest tensile stresses are to be expected. Therefore, the averaged stresses at nodes were extracted for additional post-processing directly from the ABAQUS® binary result file using another user written FORTRAN routine (stress.f in figure A1) the flow chart of which is depicted in Figure A3.

Appendix 2

Finite Element (FE) Analysis Formulation

A contact analysis was performed in order to investigate the influence of modeling the roller versus modeling the support as a simple boundary condition at one nodal point. It was expected that accounting for the roller would change the contact location and result in a shorter span, s, of the specimen and thus result in a different stress distribution along the bottom surface of the specimen. The contact analysis was performed using only two-dimensional finite element models of the specimens as shown in Figure A4a. Only 20% of the outer part of the roller was modeled with finite elements as shown in detail in Figure A4b. A roller with a diameter of 4.73 mm was modeled which corresponds to the roller diameter of the test fixture used in references 3&4. Material properties for the steel rollers used in the simulation are given in Table 1. Displacements in x and y direction were suppressed for all nodes along the inner radius of the model and along the line of symmetry of the roller to simulate the rigid behavior of the roller. Contact was modeled between two deformable bodies with small relative motion without friction using the concept of master and slave surfaces available in ABAQUS® [6]. The top surface of the elements in the refined section of the roller modeled made up the master, or target , surface as shown in Figure A4b, while the surface of the elements in the refined section at the bottom of the specimen defined the slave or contact surface used in the analysis.

Contact Analysis results

The roller support was modeled and corresponding contact analysis was performed for specimen configuration B2, only, because discrepancy in stresses between the finite element and the beam theory results were most pronounced for this configuration as shown in Figures 19-21. Additionally, the thinner 24-ply IM7/8552 B2 configuration exhibited a more pronounced non-uniform stress distribution between the inner load noses than the thick laminates. Therefore, the B2 configuration was modeled for the 24-ply and 36-ply IM7/8552 layups and the 24-ply S2/8552 layup.

Figure A5 shows the finite element mesh for the 24-ply IM7/8552 carbon/epoxy material B2 type specimen. The full specimen and the details are shown in the deformed position at the failure load. As shown in the detail of Figure A5, contact occurs only locally. Due to the local rotation of the specimen at the support, the contact location is changed and moves inward which reduces the effective span s by about 0.6 mm at each support.

The tension stresses computed at the bottom of the specimen, using 2D contact analysis where the roller support were modeled, are shown in Figures A6 a-c. The difference between the beam theory and FE stresses for all configurations are lower compared to results obtained from analysis where simple supported boundary conditions had been used. This may be explained by considering equation (2). Because the distance between the load points (s-ℓ) remains unchanged in the simulation, the reduction of the effective span, s, causes the same reduction in the length, ℓ , which is used in equation (2) to

calculate the stresses. For all configurations investigated, the discrepancy between the FE and beam theory results became smaller (max. 3%) when the rollers were modeled in conjunction with contact analysis instead of simple supported boundary conditions.

TABLE I. MATERIAL PROPERTIES.

S2/8552 Unidirectional Glass-Epoxy Prepreg		
E_{11} = 47.71 GPa	E_{22} = 12.27 GPa	E_{33} = 12.27 GPa
ν_{12} = 0.278	ν_{13} = 0.278	ν_{23} = 0.403
G_{12} = 4.83 GPa	G_{13} = 4.83 GPa	G_{23} = 4.48 GPa
IM7/8552 Unidirectional Carbon-Epoxy Prepreg		
E_{11} = 161.0 GPa	E_{22} = 11.38 GPa	E_{33} = 11.38 GPa
ν_{12} = 0.32	ν_{13} = 0.32	ν_{23} = 0.436
G_{12} = 5.17 GPa	G_{13} = 5.17 GPa	G_{23} = 3.98 GPa
Steel		
E = 210.0 GPa		ν = 0.3

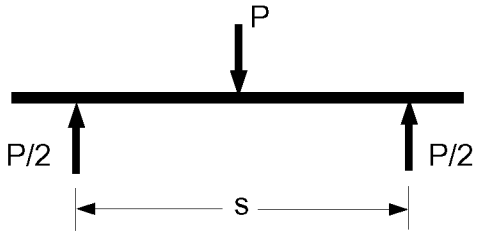

Configuration	s, mm
A	25.4
B	50.8
C	76.2

(a) 3-point bending

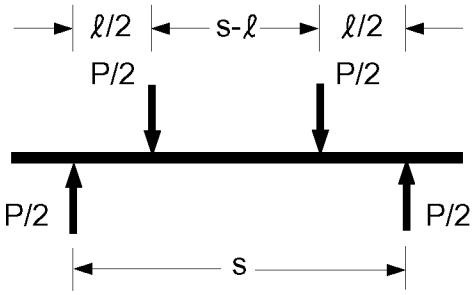

Config.	s, mm	ℓ/2, mm	s-ℓ, mm
A1	50.8	12.7	25.4
A2	76.2	25.4	25.4
B2	76.2	12.7	50.8
B3	102	25.4	50.8

(b) 4-point bending

Figure 1. Bending test configurations.

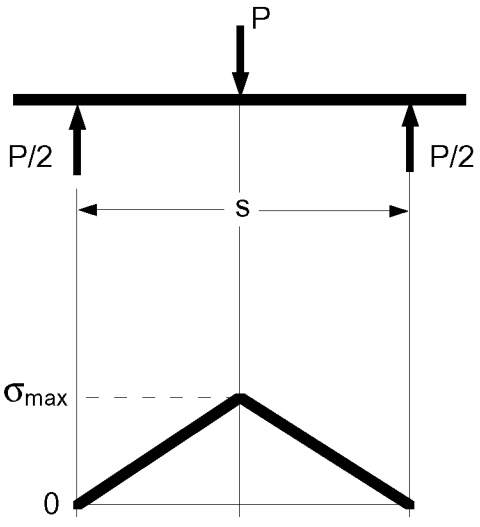

(a) 3-point bending

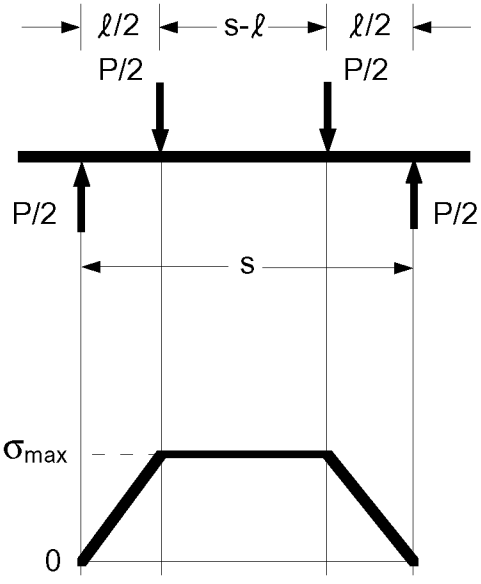

(b) 4-point bending

Figure 2. Beam theory tension stress distribution on the bottom of beam.

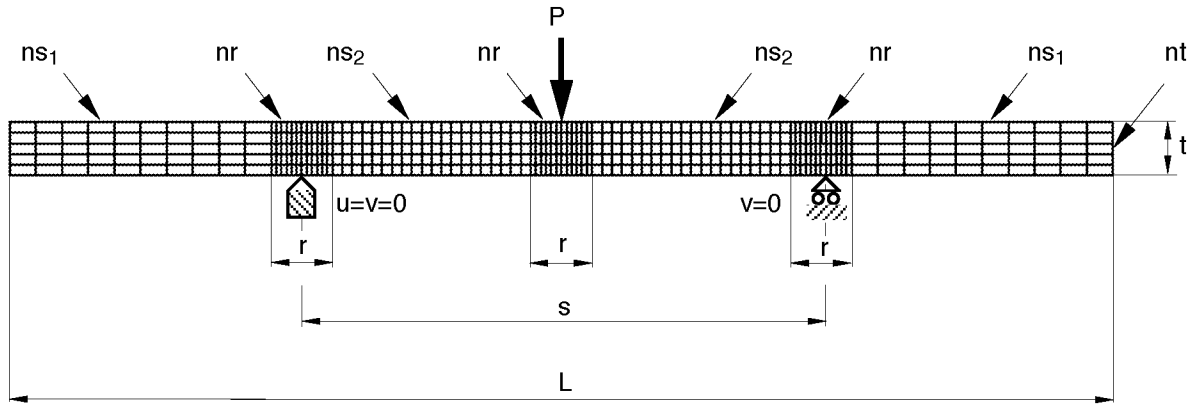

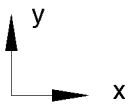

L: total specimen length
s: span between supports
r: length of refined section around supports and load points
t: specimen thickness
nr: number of elements in refined section
ns_1: number of elements in overhang
ns_2: number of elements in section between support and load point
nt: number of elements over the thickness

(a) Two dimensional FE model of three point bending specimen

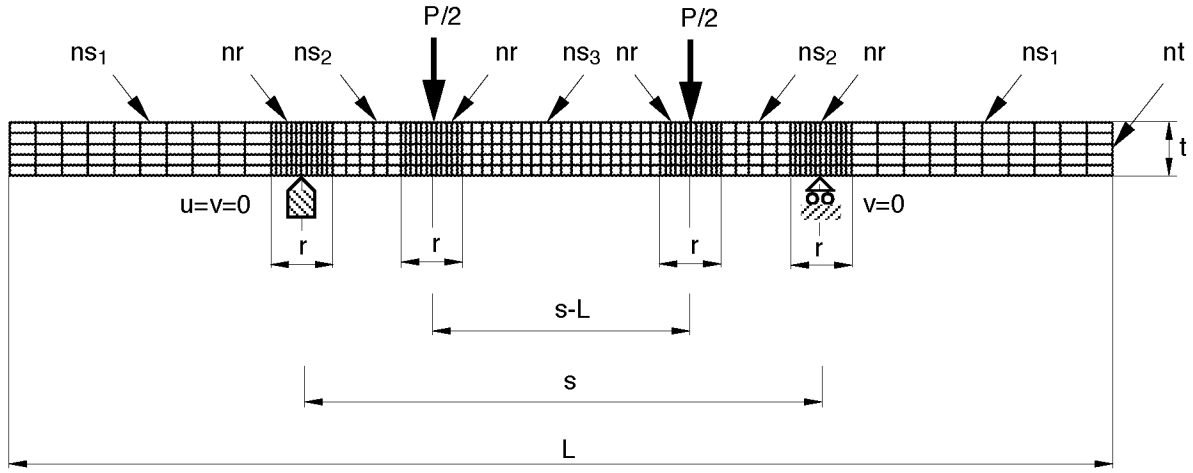

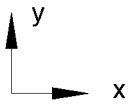

s-L: span between inner load points
ns_3: number of elements in the center section

(b) Two dimensional FE model of four point bending specimen

Figure 3. Two dimensional FE models and corresponding load and boundary conditions

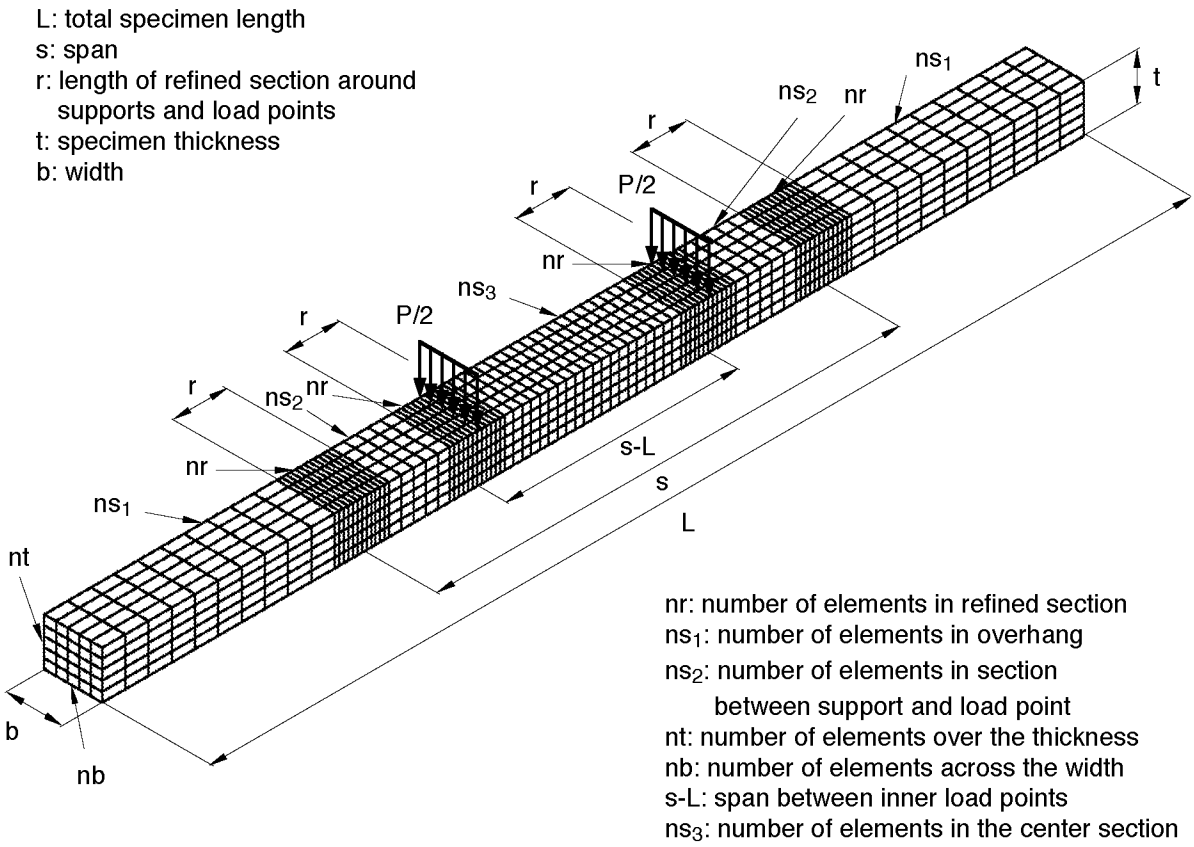

Figure 4. Three dimensional FE model of four point bending specimen.

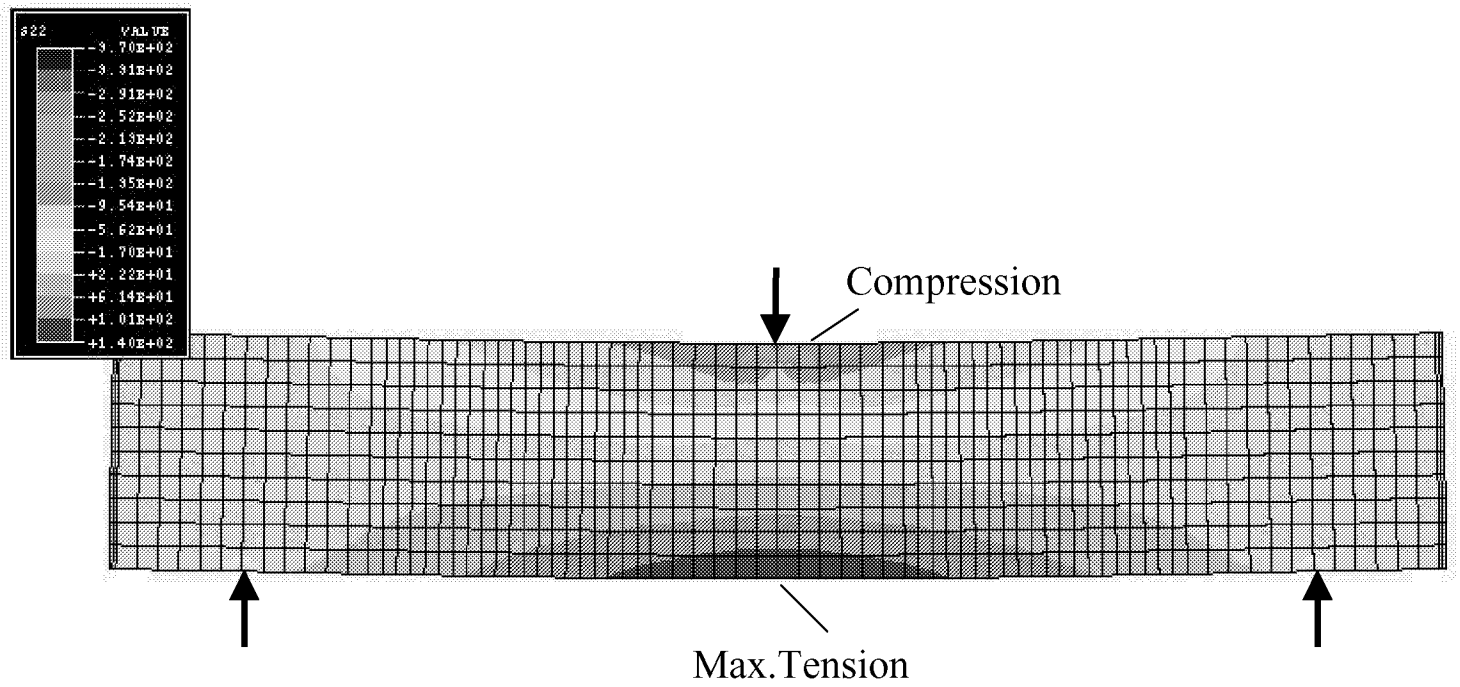

Fig. 5 Finite Element Mesh showing Deformed Geometry and Bending Stresses for S2/8552 Glass Epoxy 3-Point Bend Configuration A

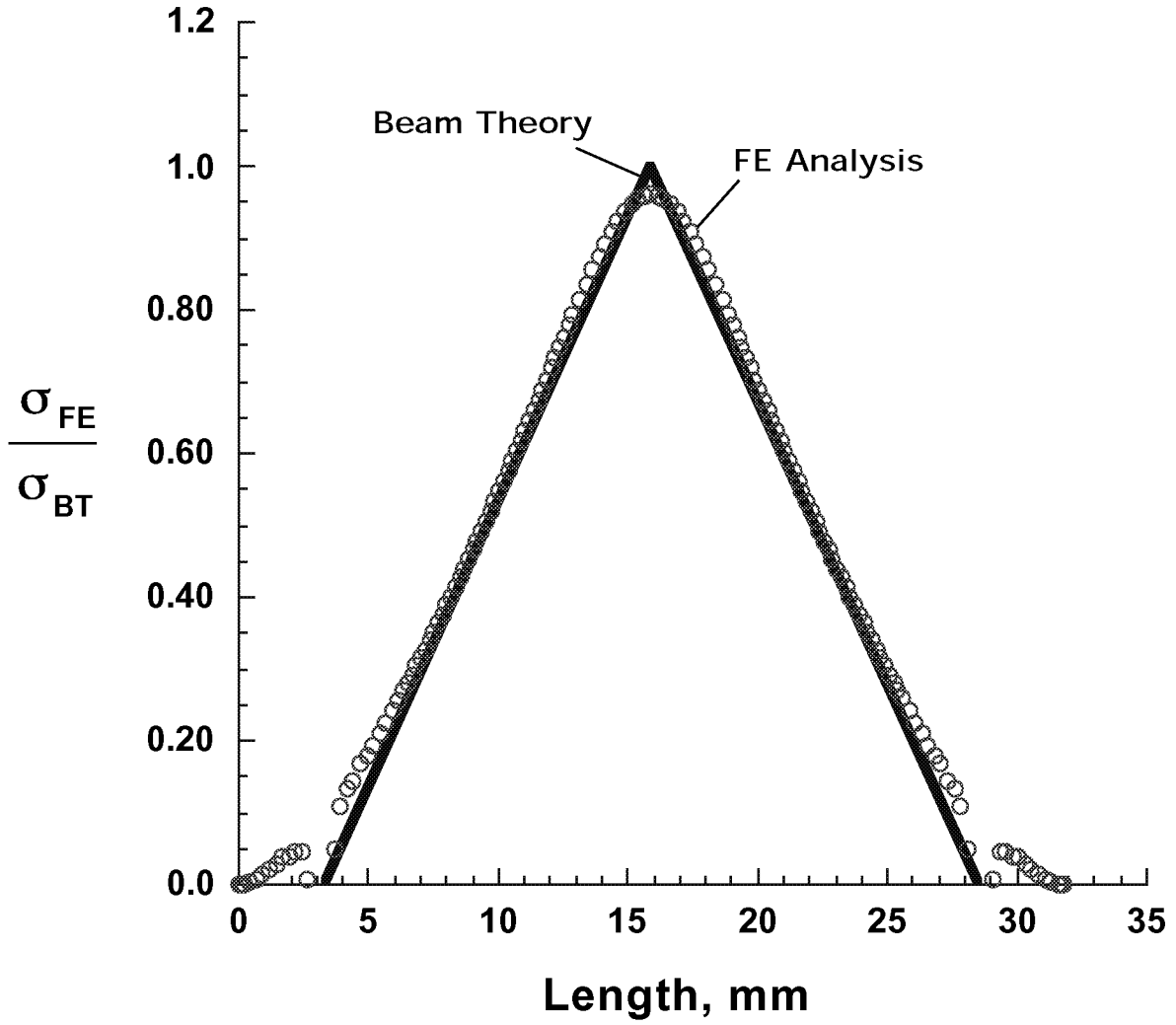

Fig.6 Normalized Tension Stress Distribution from 2D Plane-Strain Linear FE Analysis S2/8552 Glass-epoxy 3-point bending Configuration A

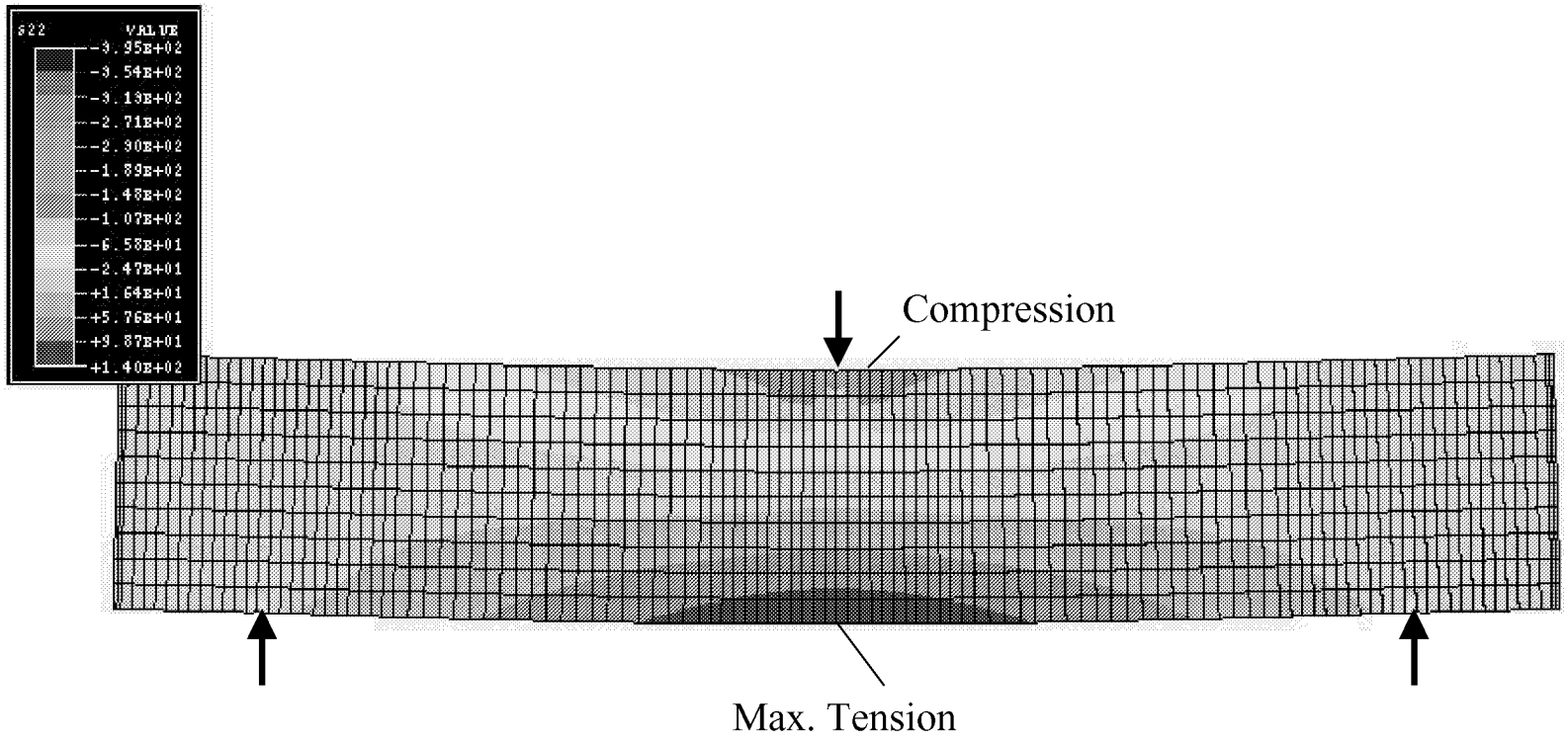

Fig.7 Finite Element Fine Mesh showing Deformed Geometry and Bending Stresses for S2/8552 Glass Epoxy 3-Point Bend Configuration A

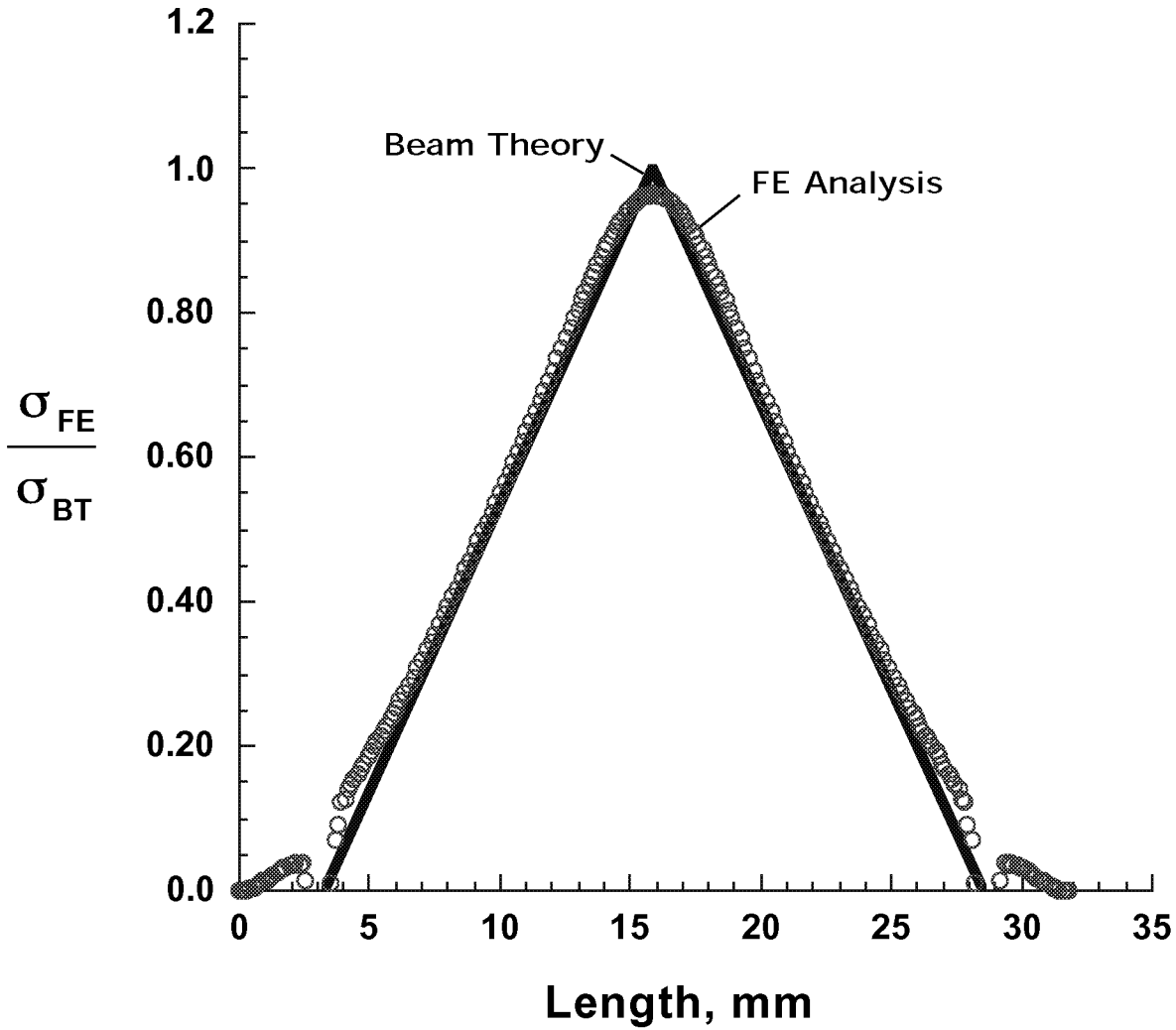

Fig.8 Normalized Tension Stress Distribution from 2D Plane-Stress non-linear FE Analysis Fine Mesh for S2/8552 Glass-epoxy 3-Point Bending Configuration A

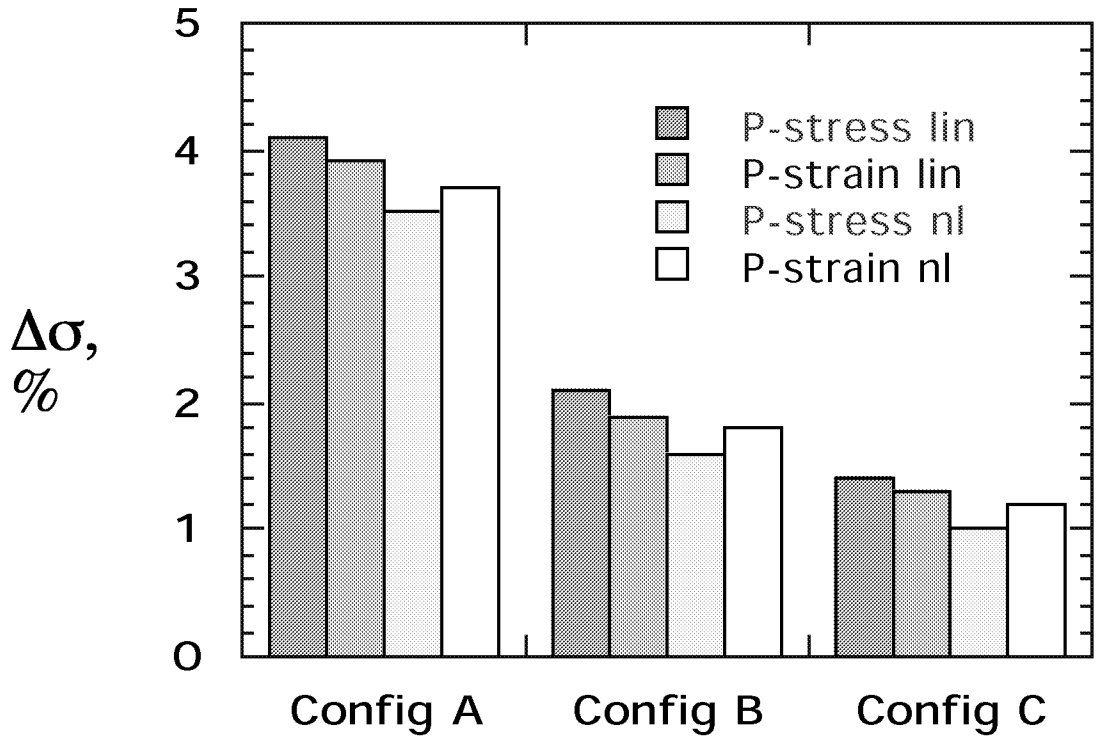

Fig.9 Comparison of Discrepancy between Beam Theory and FE analysis
S2/8552 Glass-epoxy, 3-point bending configurations

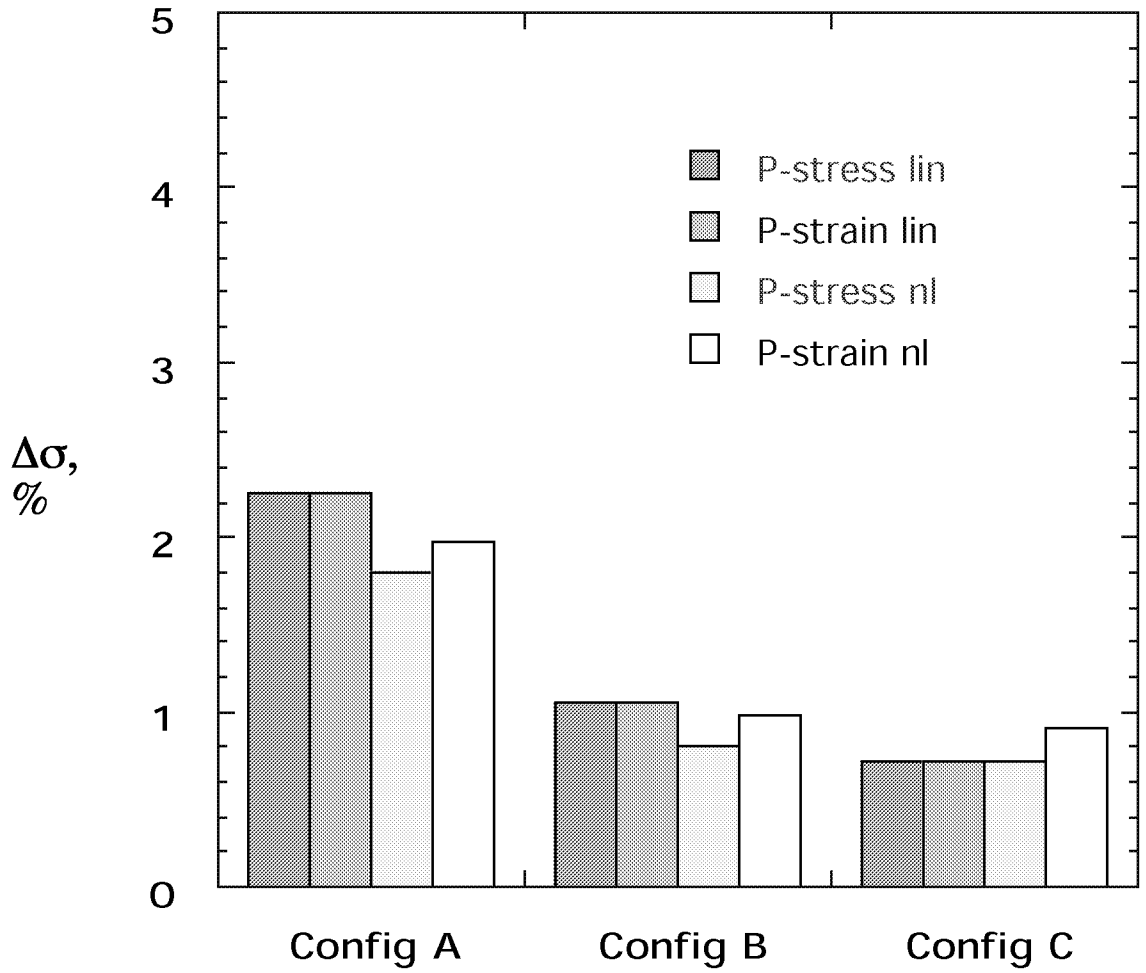

Fig.10 Comparison of Discrepancy between Beam Theory and FE analysis
24-ply IM7/8552 Carbon-epoxy, 3-point bending configurations

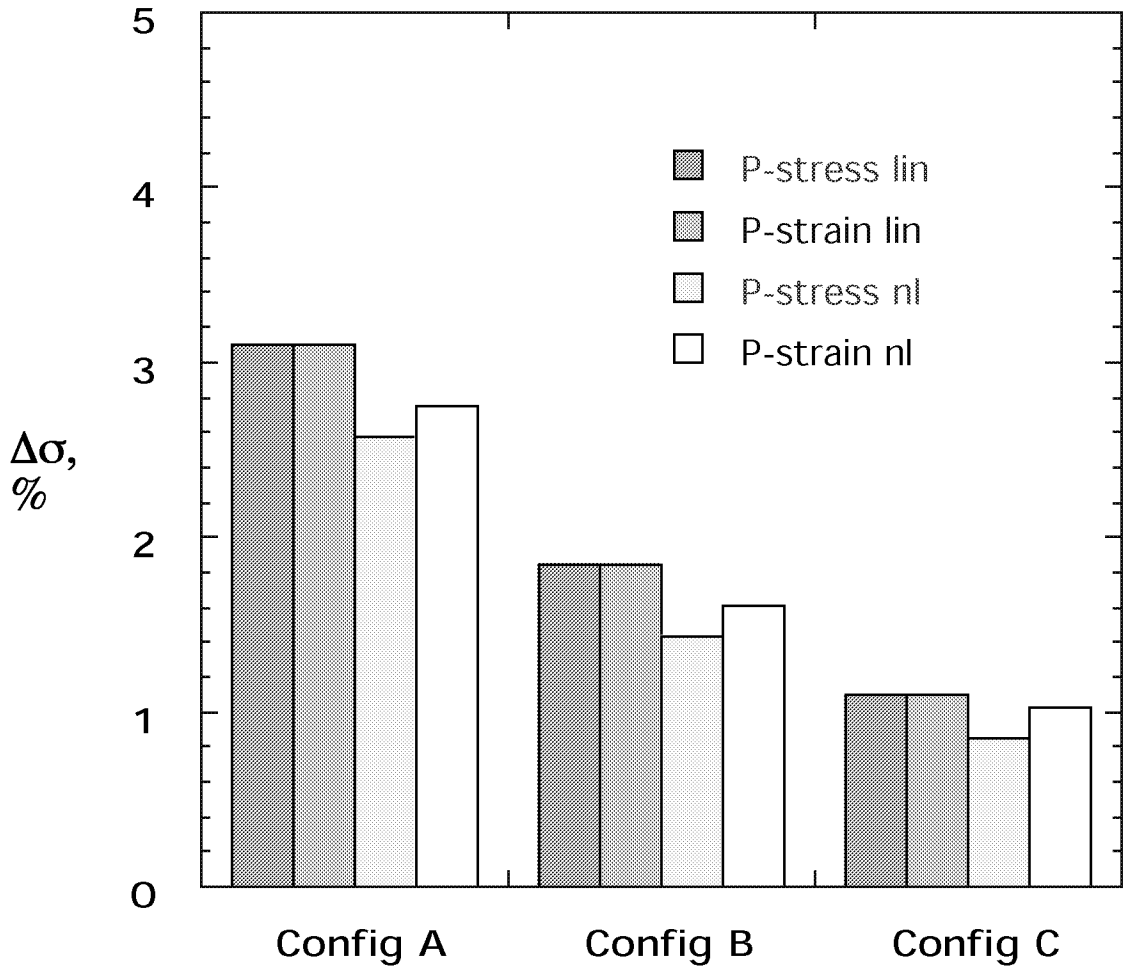

Fig.11 Comparison of Discrepancy between Beam Theory and FE analysis
36-ply IM7/8552 Carbon-epoxy, 3-point bending configurations

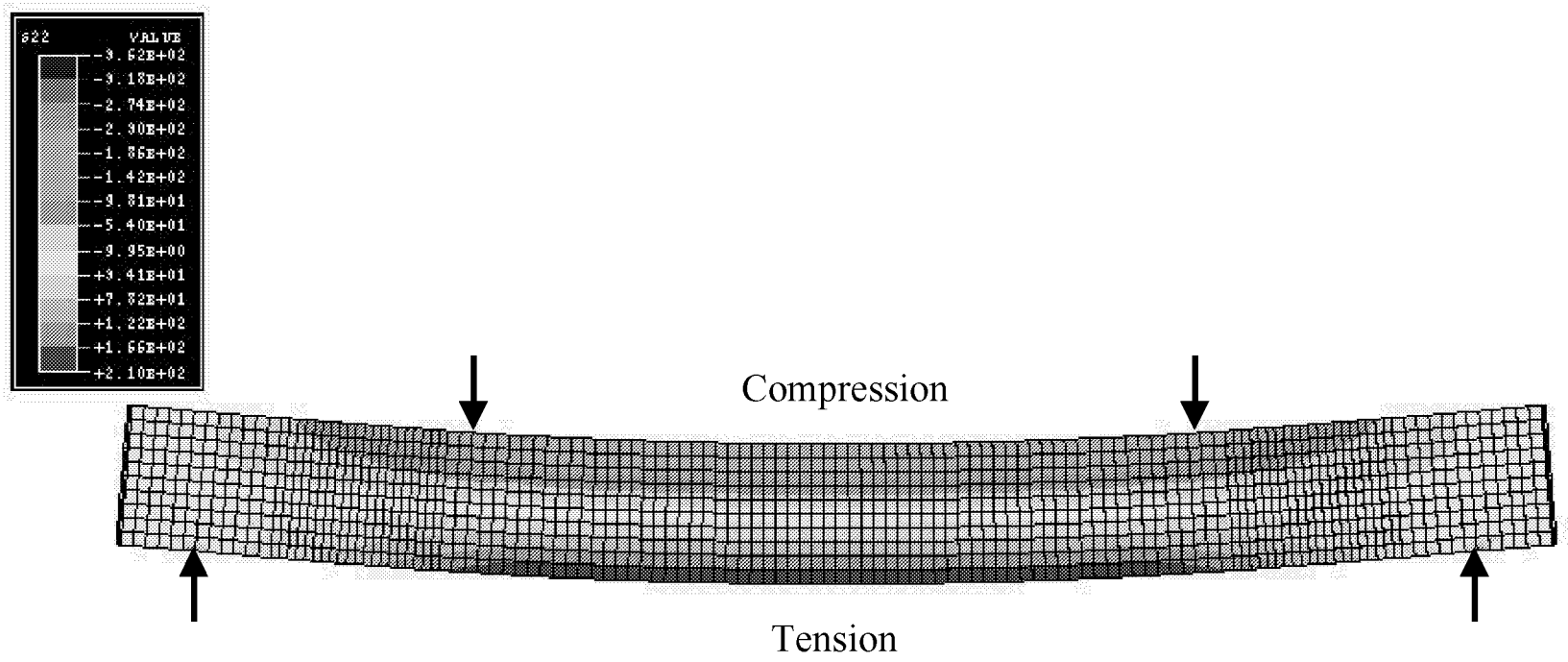

Fig.12 Finite Element Mesh showing Deformed Geometry and Bending Stresses for S2/8552 Glass Epoxy 4-Point Bend configuration A1

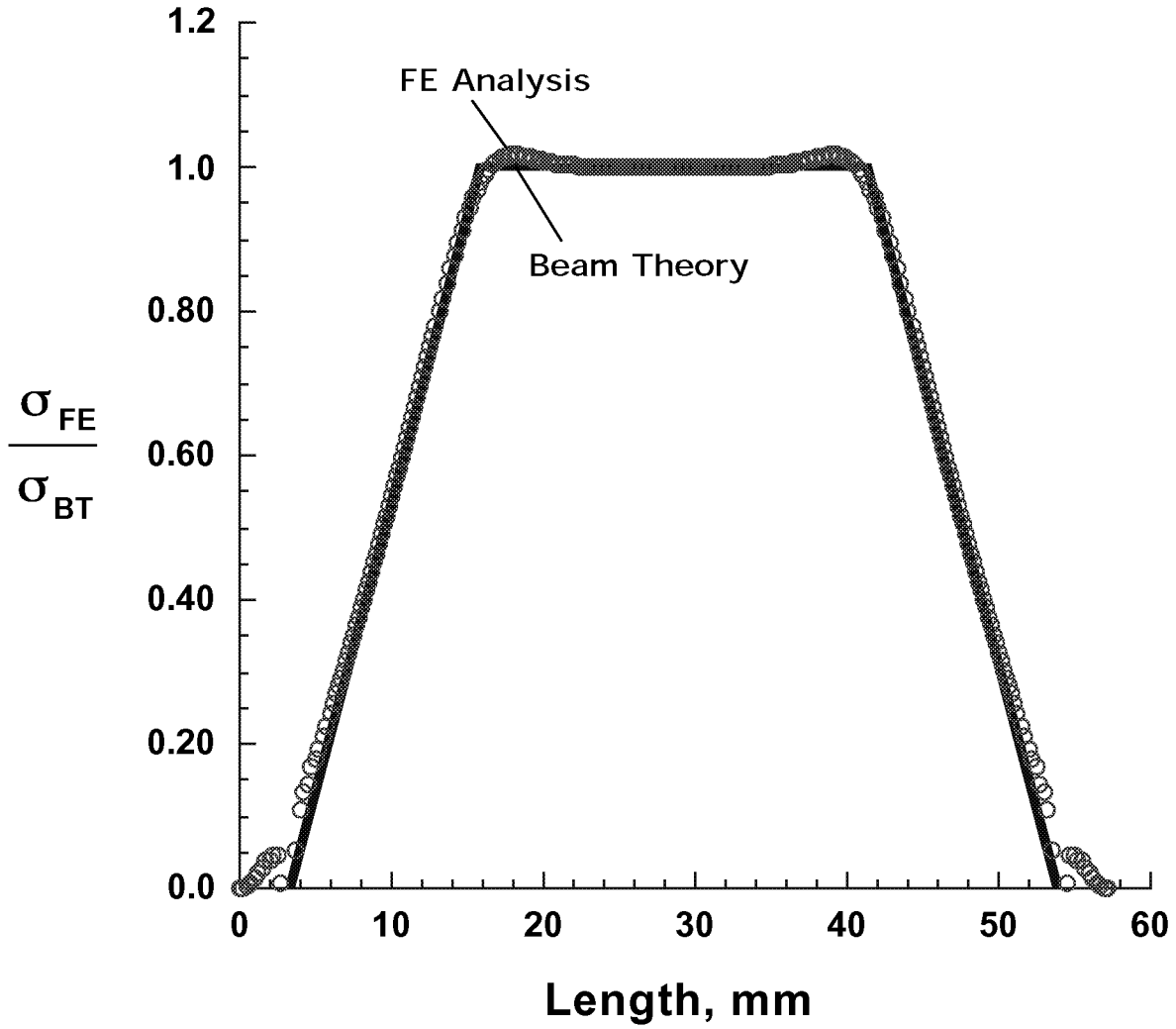

Fig.13 Normalized Tension Stress Distribution from 2D Plane-Strain Linear FE Analysis S2/8552 Glass-epoxy 4-point bending Configuration A1

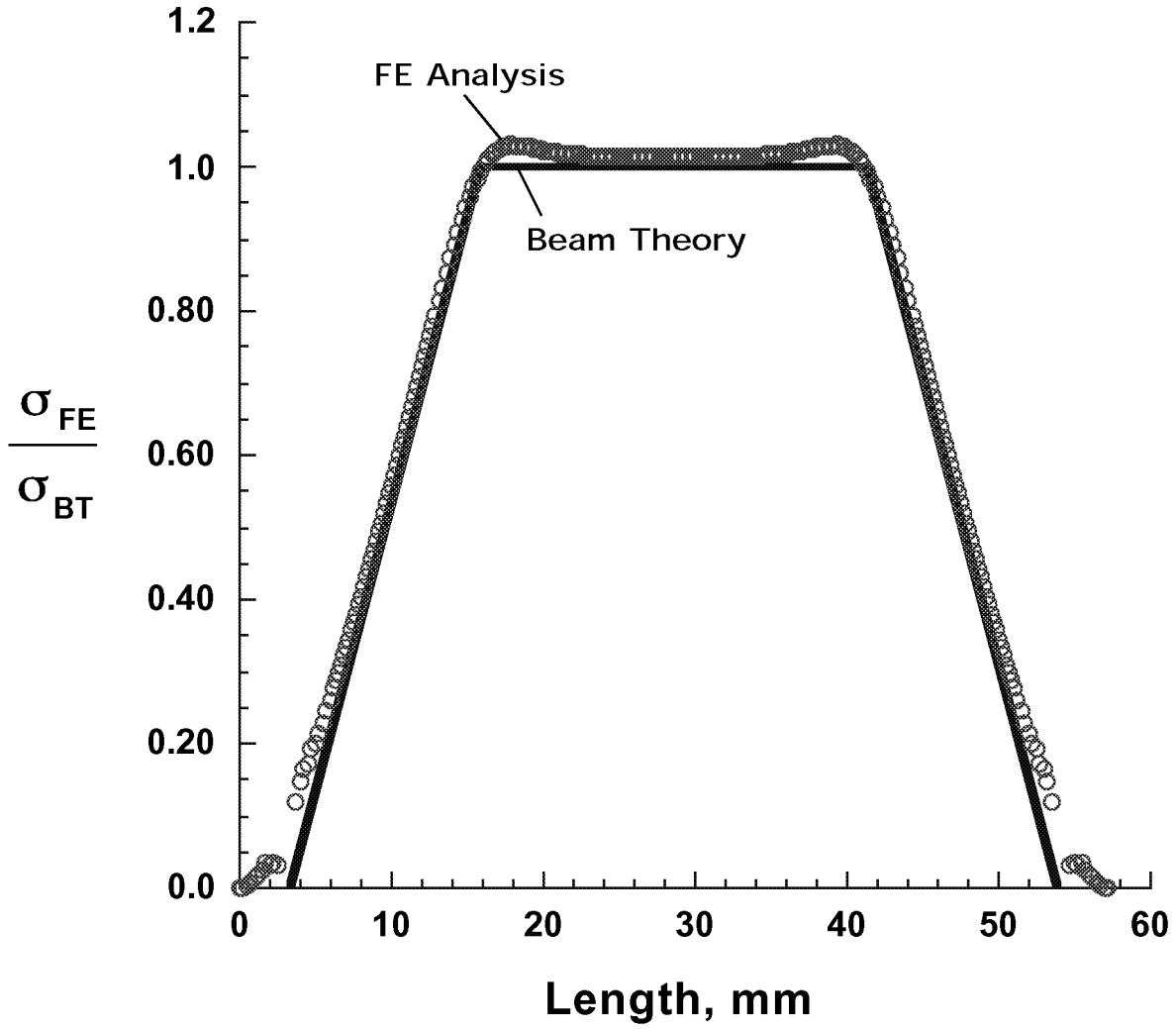

Fig.14 Normalized Tension Stress Distribution from 2D Plane-Strain non-linear FE Analysis S2/8552 Glass-epoxy 4-point bending Configuration A1

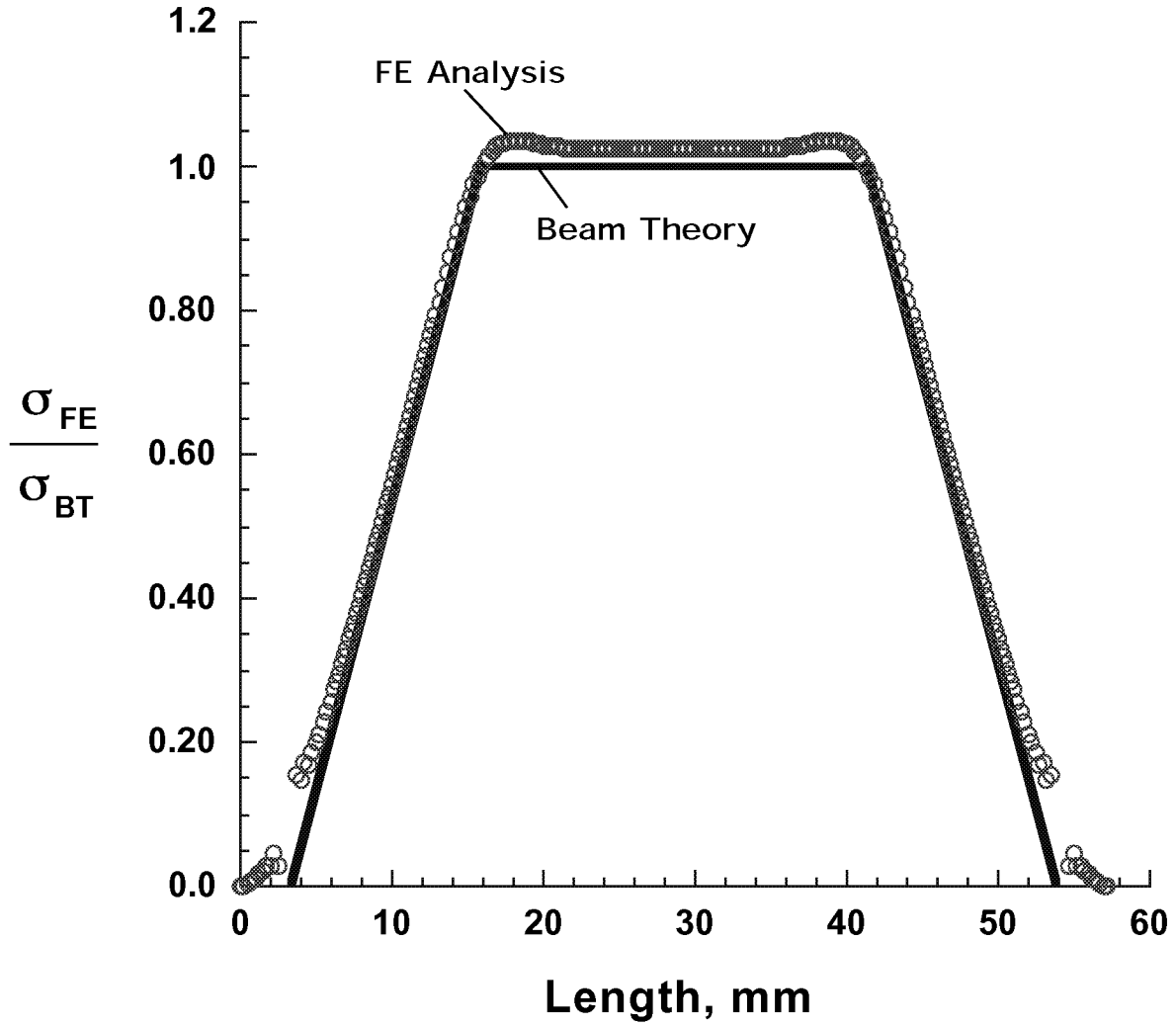

Fig.15 Normalized Tension Stress Distribution from 2D Plane-Stress non-linear FE Analysis S2/8552 Glass-epoxy 4-point bending Configuration A1

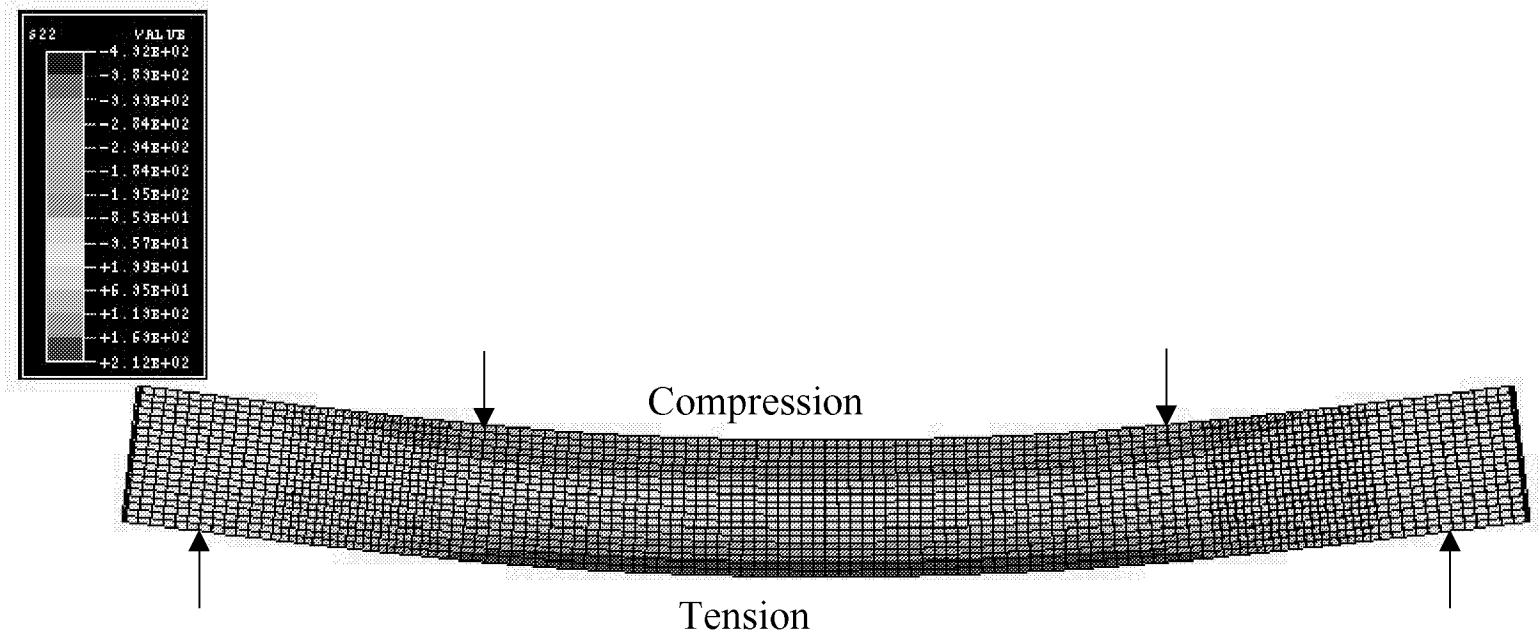

Fig. 16 Finite Element Fine Mesh showing Deformed Geometry and Bending Stresses for S2/8552 Glass Epoxy, 4-Point Bend configuration A1

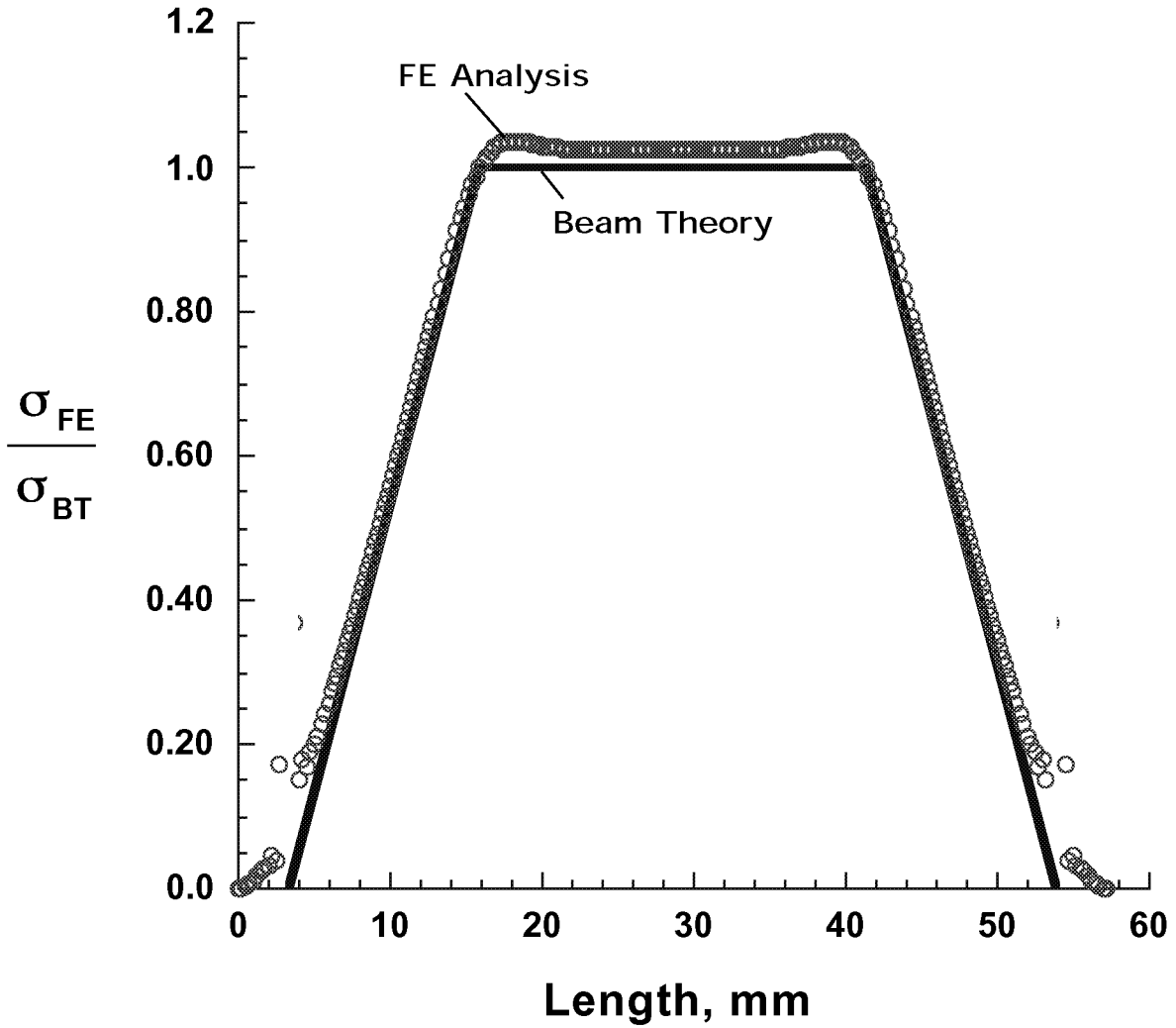

Fig.17 Normalized Tension Stress Distribution from 2D Plane-Stress non-linear FE Analysis Fine Mesh for S2/8552 Glass-epoxy 4-point bending Configuration A1

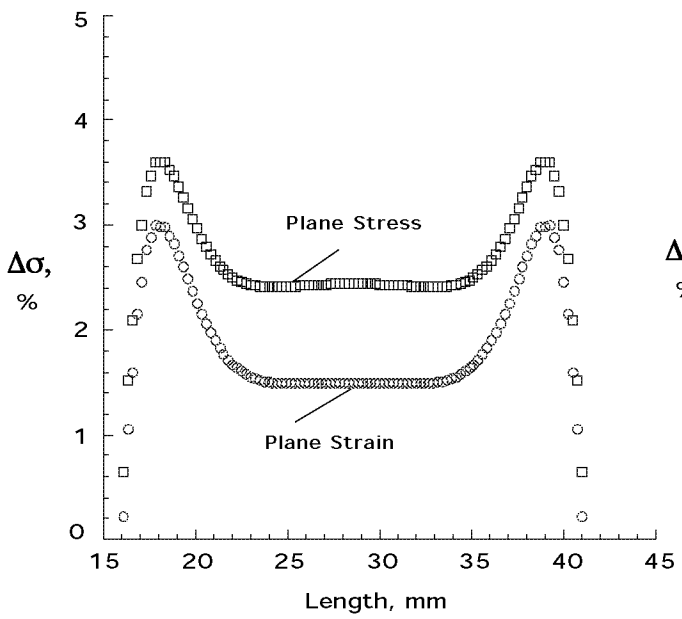

(a) Configuration A1

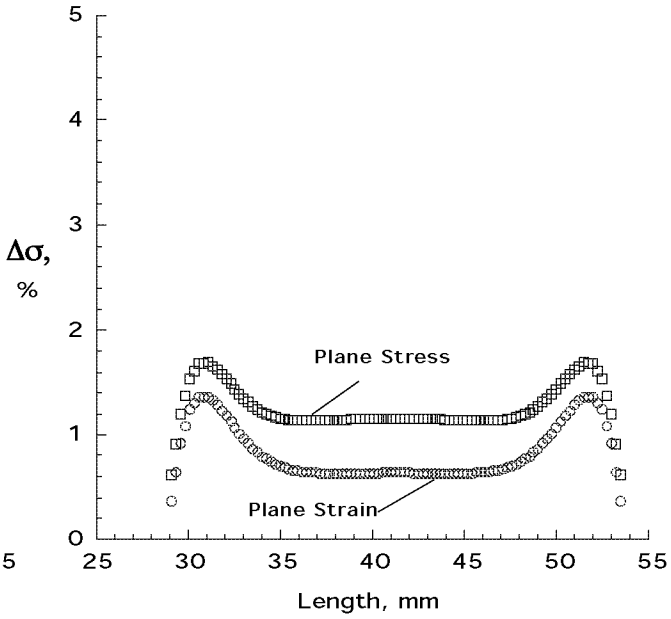

(b) Configuration A2

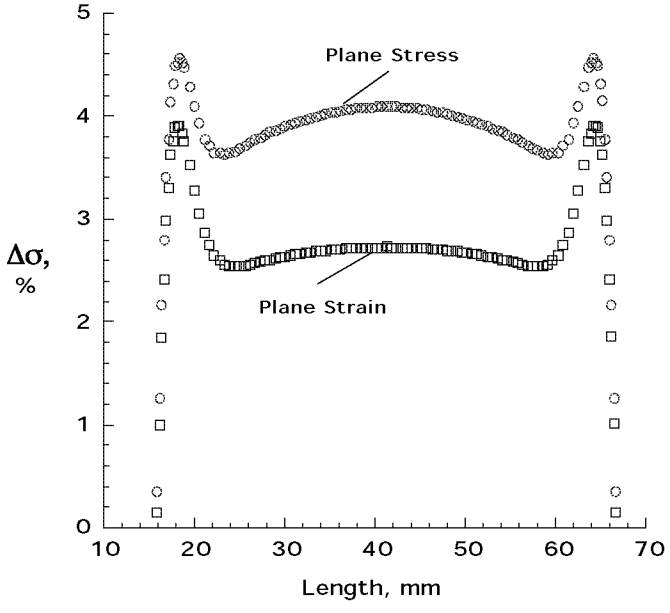

(c) Configuration B2

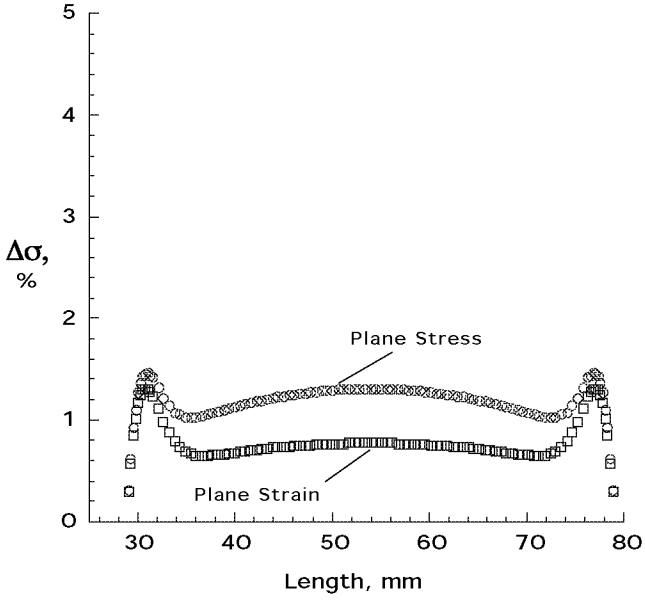

(d) Configuration B3

Fig.18 Comparison of Discrepancy between Beam Theory and Plane-Stress and Plane-Strain FE Analysis for S2/8552 Glass-epoxy 4-point bending configurations

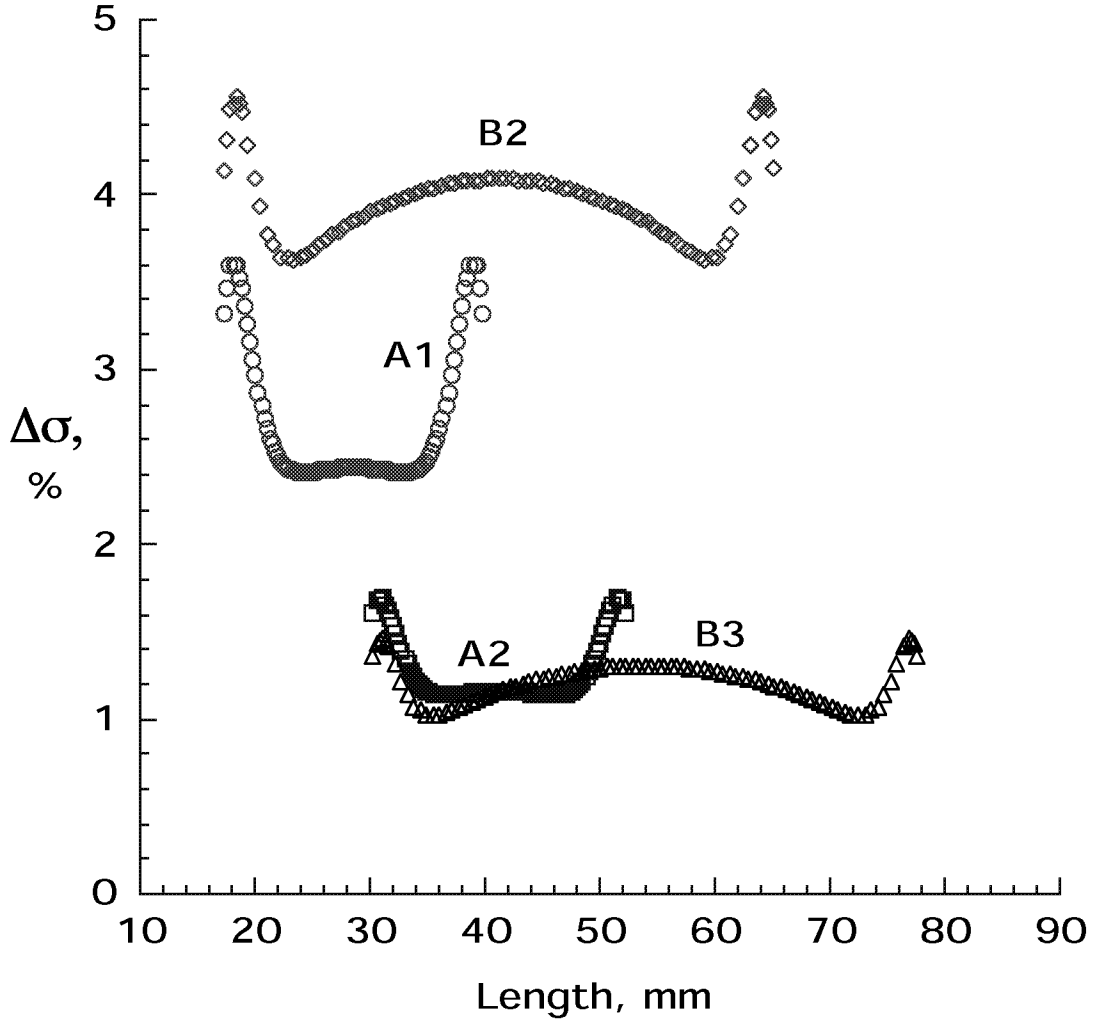

Fig.19 Comparison of Discrepancy between Beam Theory and 2D Plane-Stress non-linear FE analysis for S2/8552 Glass-epoxy 4-point bending Configurations

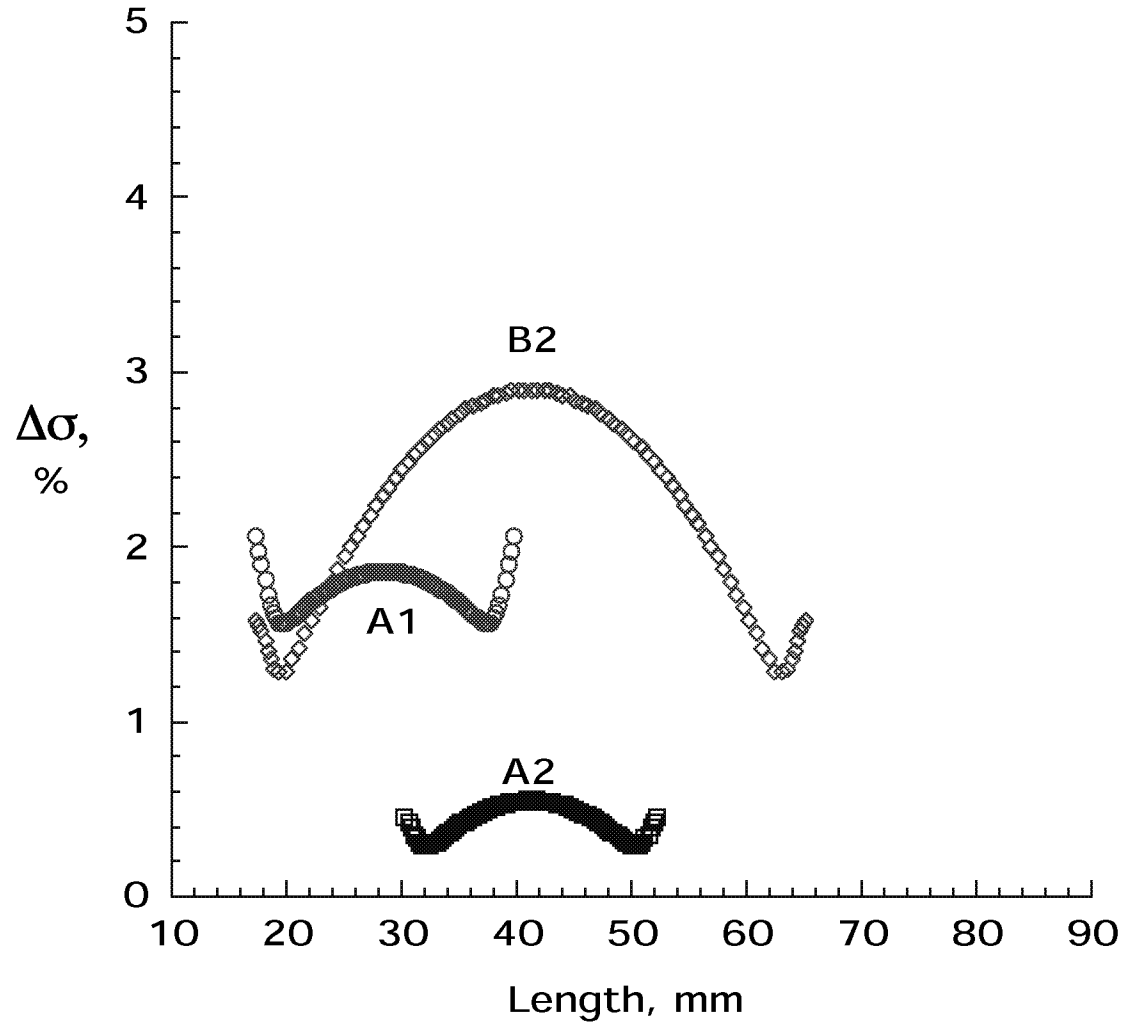

Fig.20 Comparison of Discrepancy between Beam Theory and 2D Plane-Stress non-linear FE analysis for 24-ply IM7/8552 Carbon-epoxy 4-point bending Configurations

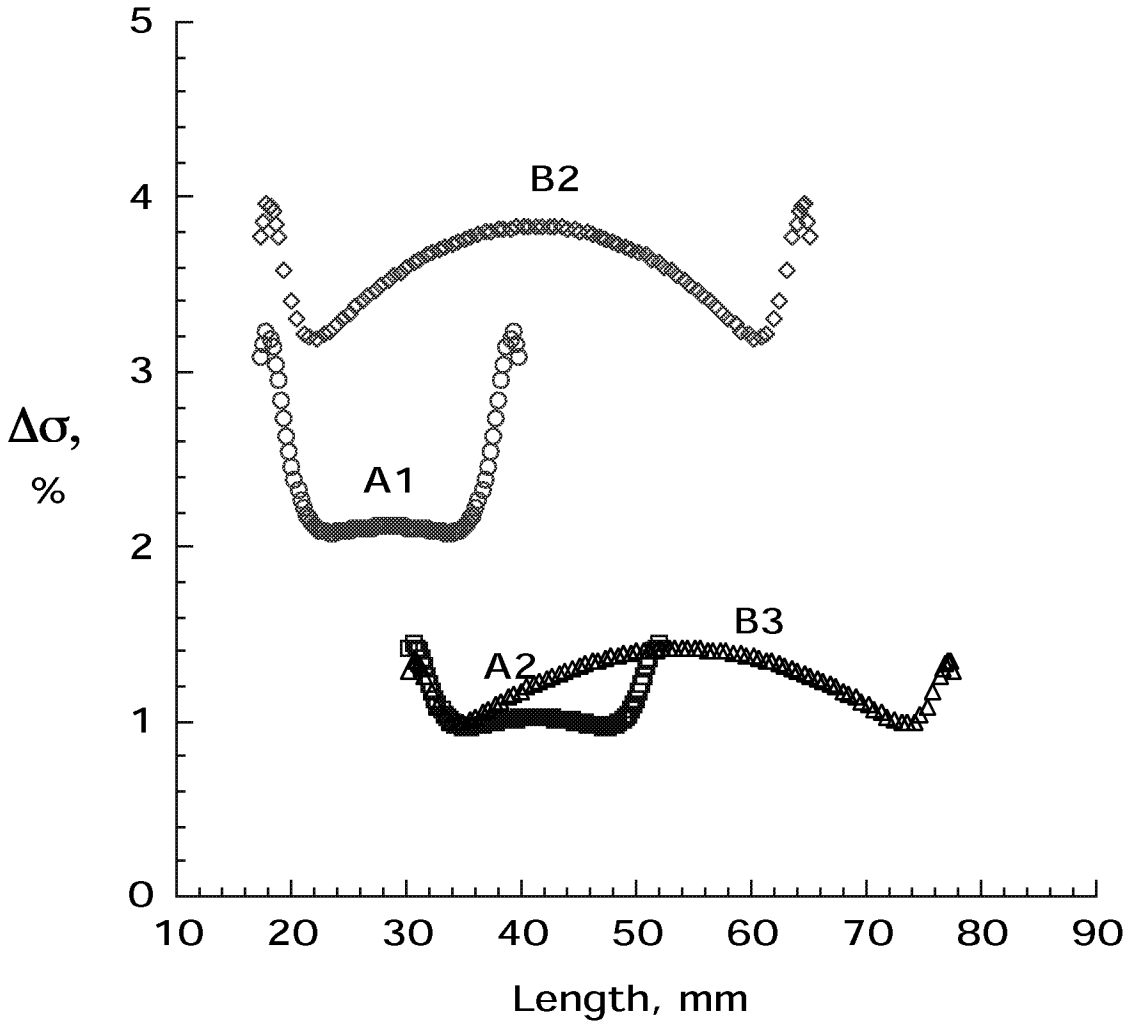

Fig.21 Comparison of Discrepancy between Beam Theory and 2D Plane-Stress non-linear FE analysis for 36-ply IM7/8552 Carbon-epoxy 4-point bending Configurations

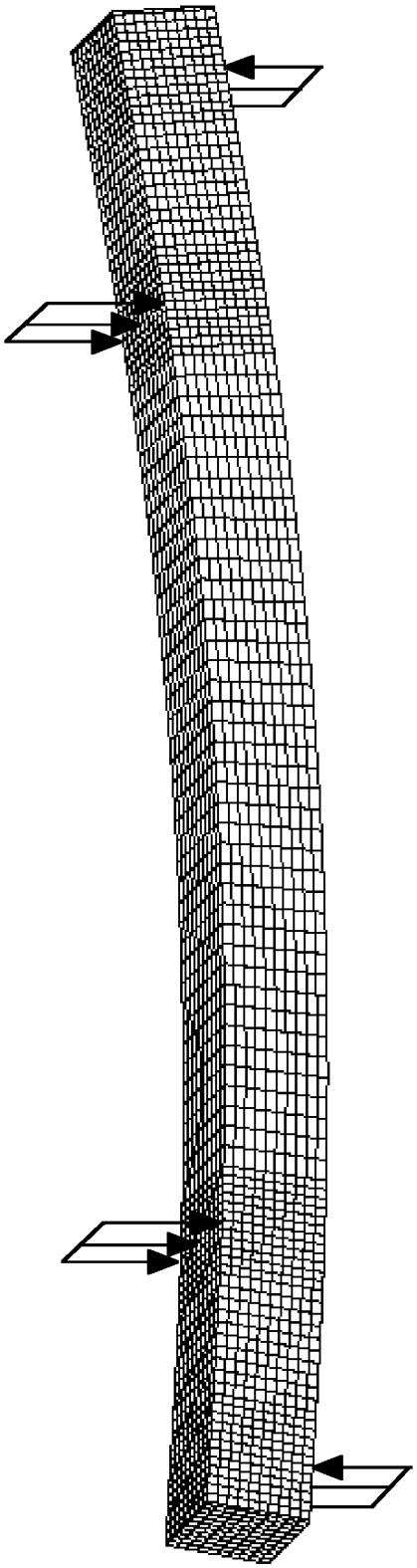

Fig. 22 Deformed 3D FE model, S2/8552, Configuration B2

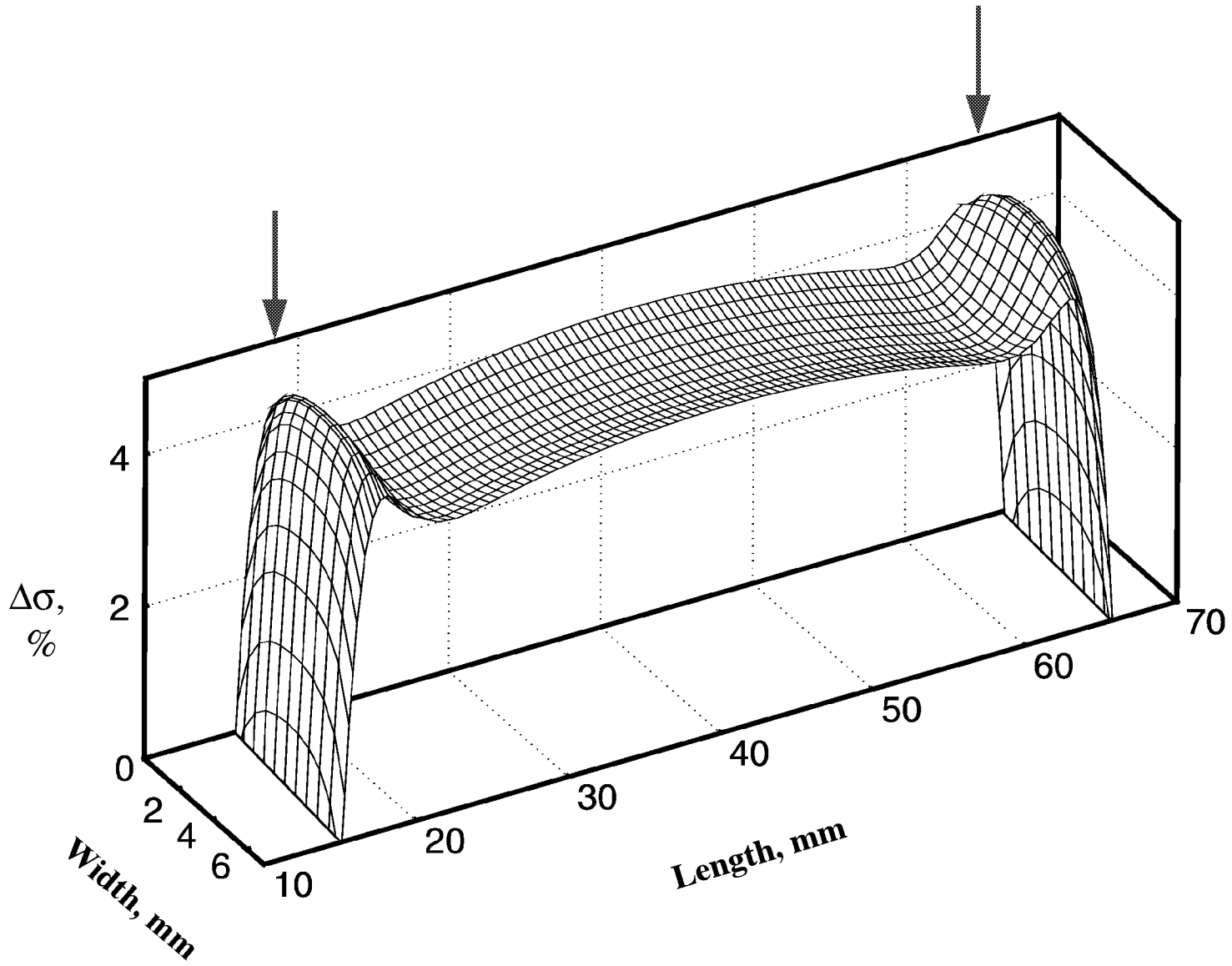

Fig. 23 Comparison of Discrepancy between Beam Theory and 3D FE analysis, S2/8552 Configuration B2

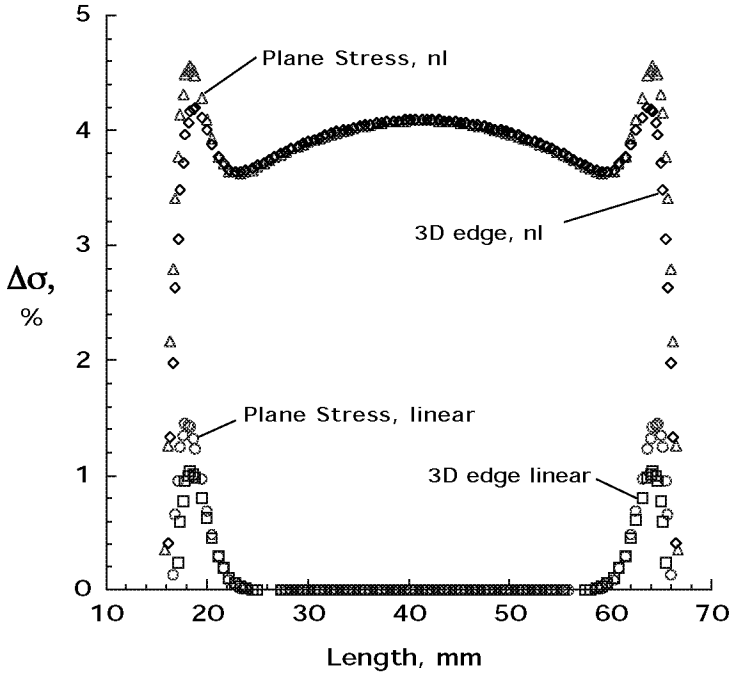

(a) 2D Plane Stress vs. 3D Edge results

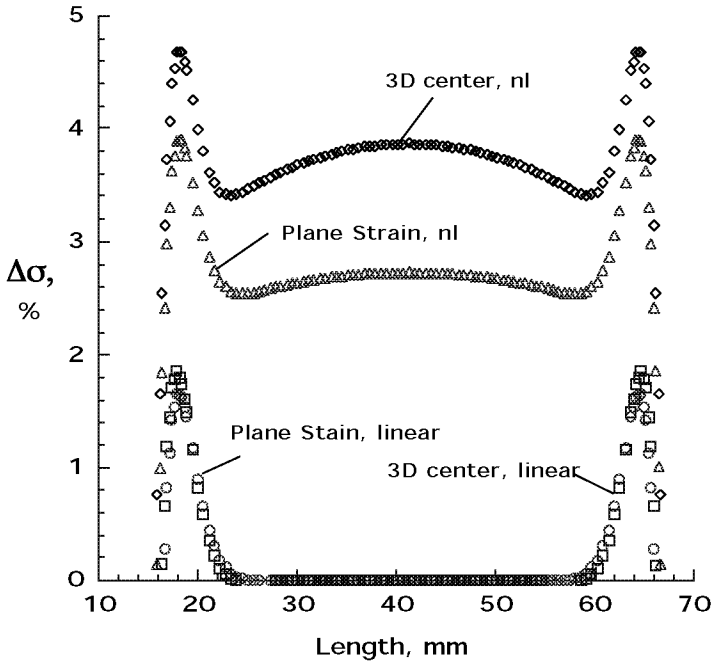

(b) 2D Plane Strain vs. 3D Center results

Fig.24 Comparison of Discrepancy between Beam Theory and 2D and 3D FE Analysis for S2/8552 Glass-epoxy 4-point bending Configuration B2

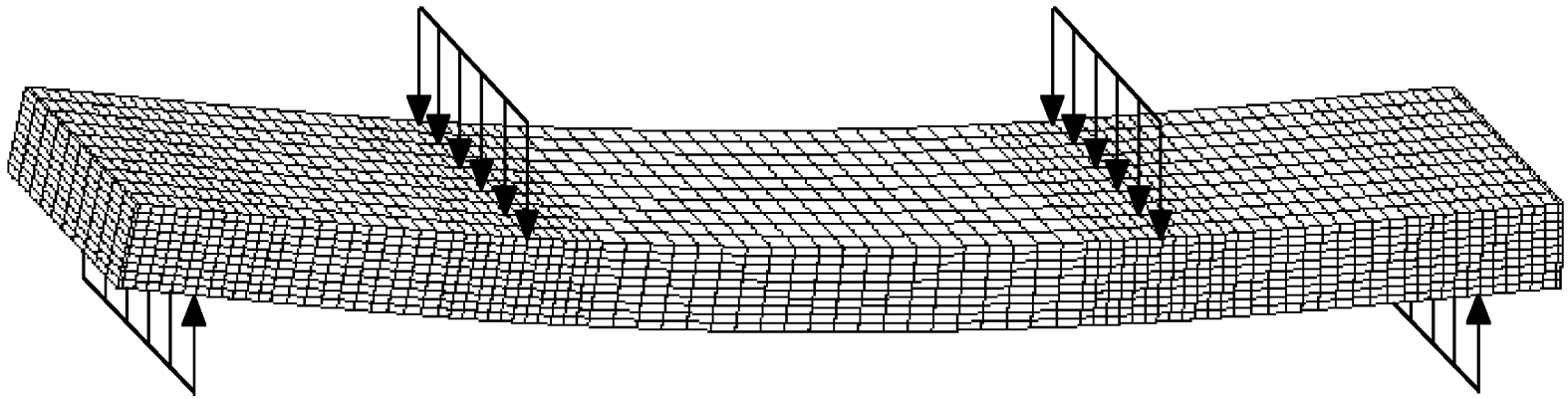

Fig. 25 Deformed 3D FE model, IM7/8552, 24 Ply Configuration A1w

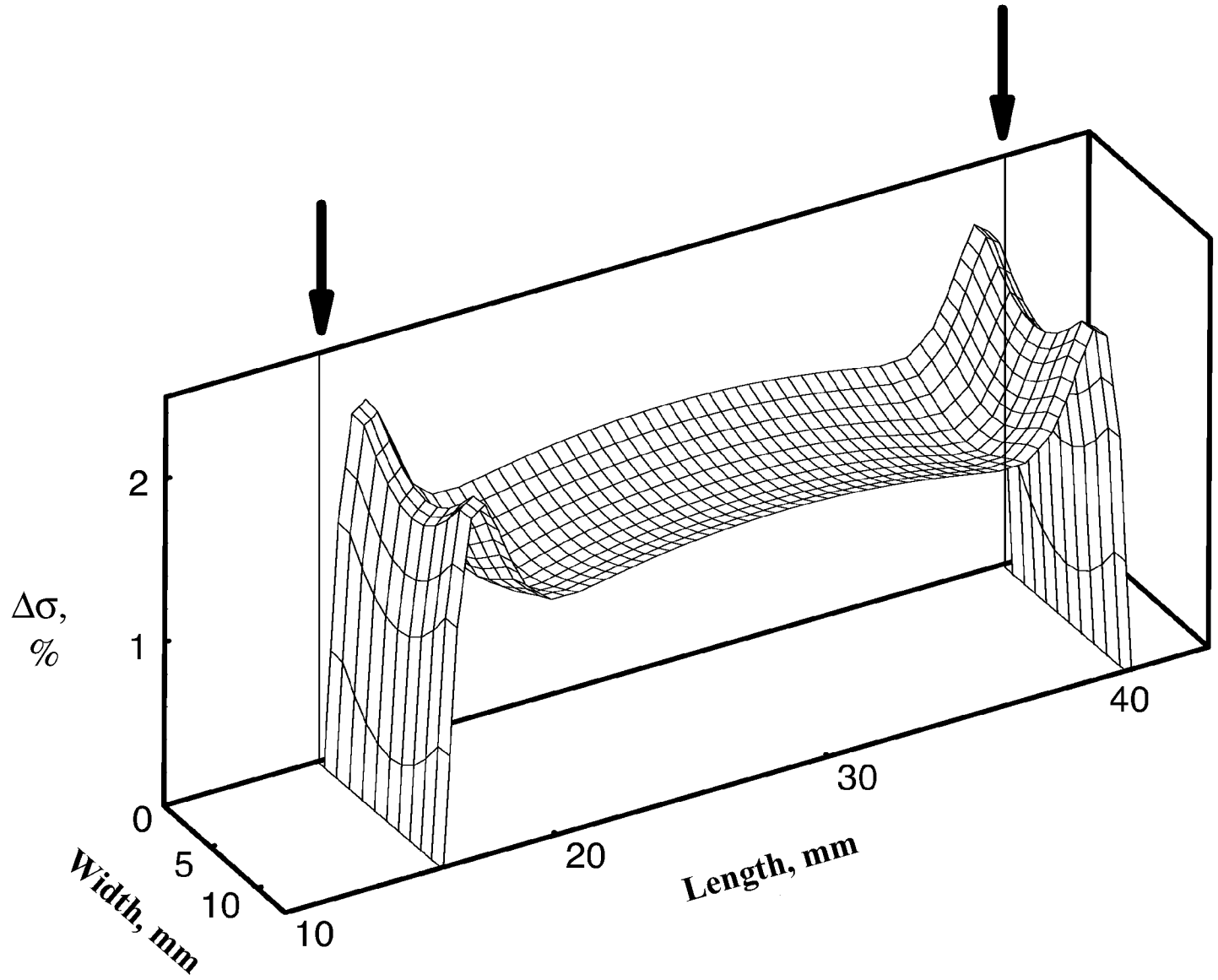

Fig. 26 Beam Theory vs. 3D Finite Element - IM7/8552 Configuration A1

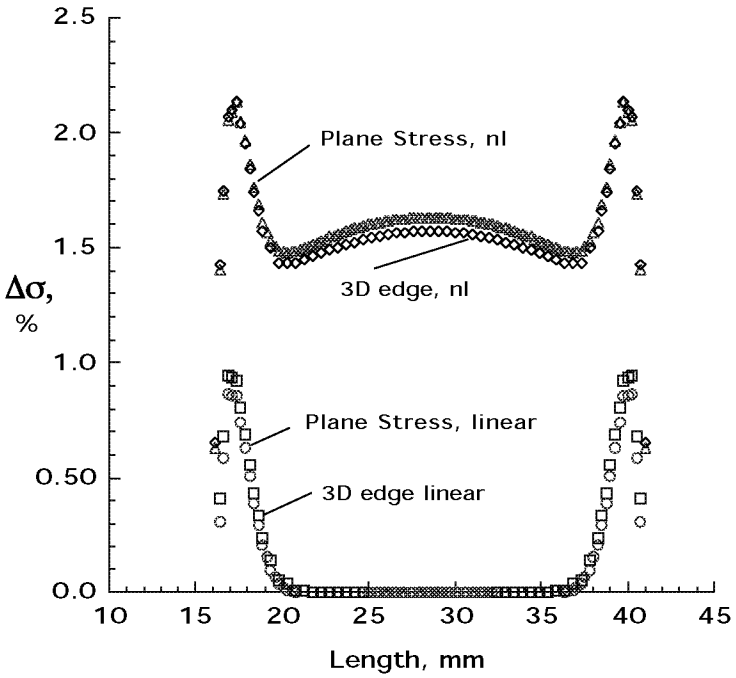

(a) 2D Plane Stress vs. 3D Edge results

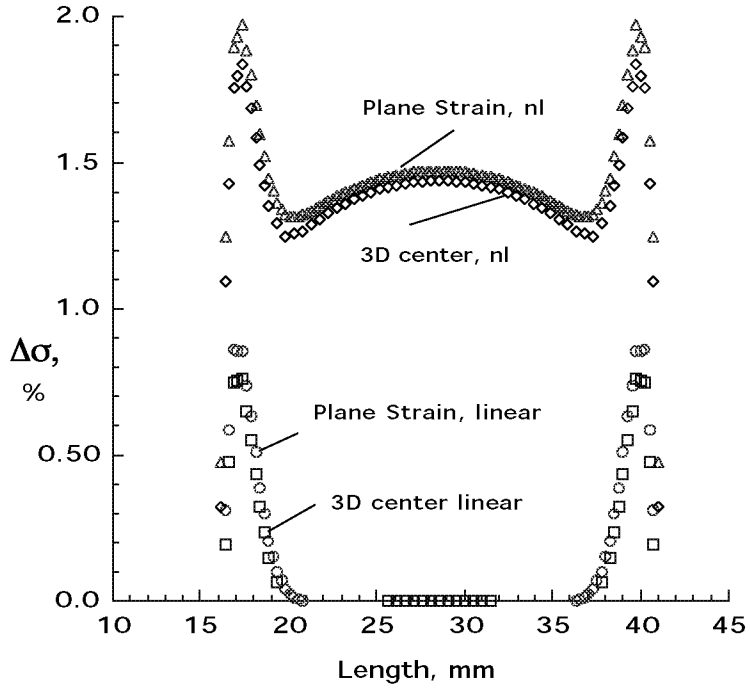

(b) 2D Plane Strain vs. 3D Center results

Fig.27 Comparison of Discrepancy between Beam Theory and 2D and 3D FE Analysis, 24-ply IM7/8552 Carbon-epoxy 4-point bending Configuration A1

Conf. A

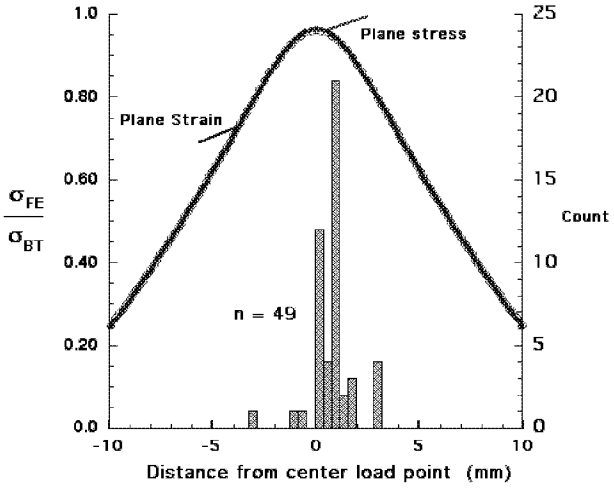

Conf. B

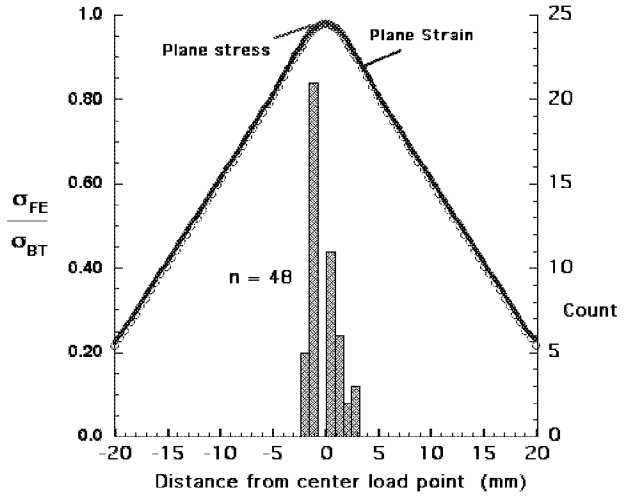

Conf. C

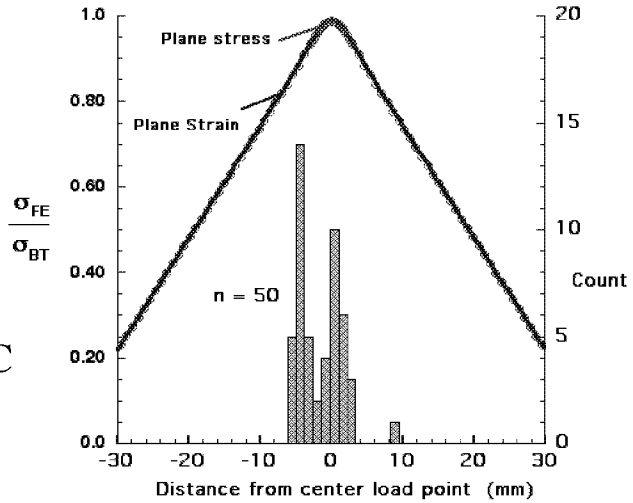

Fig.28 Comparison of Normalized Bending Stress and Failure Location S2/8552 3-point bending Configurations

Conf. A

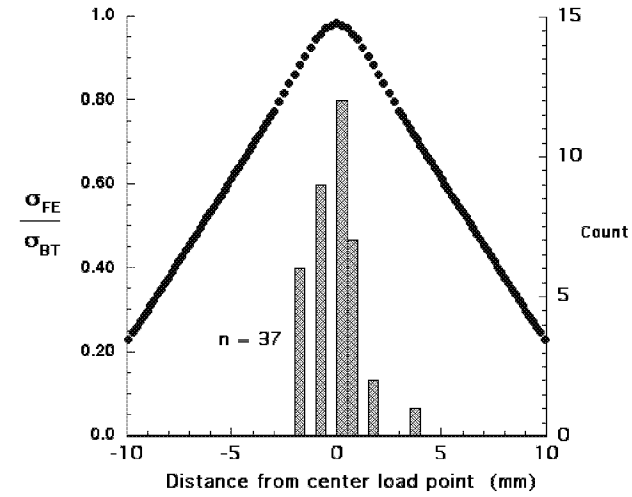

Conf. B

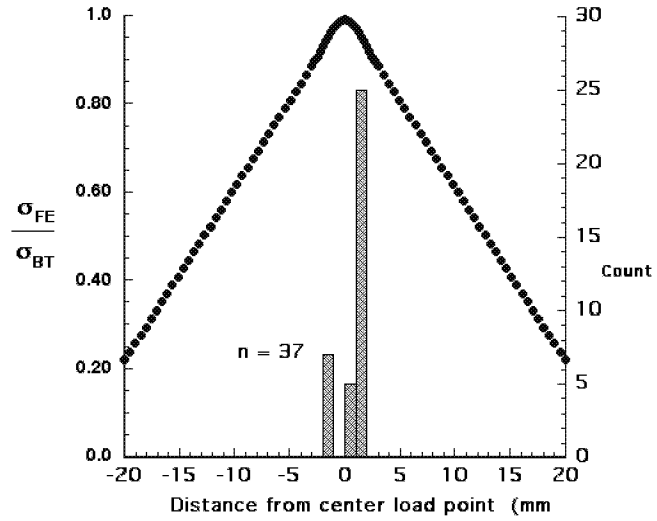

Conf. C

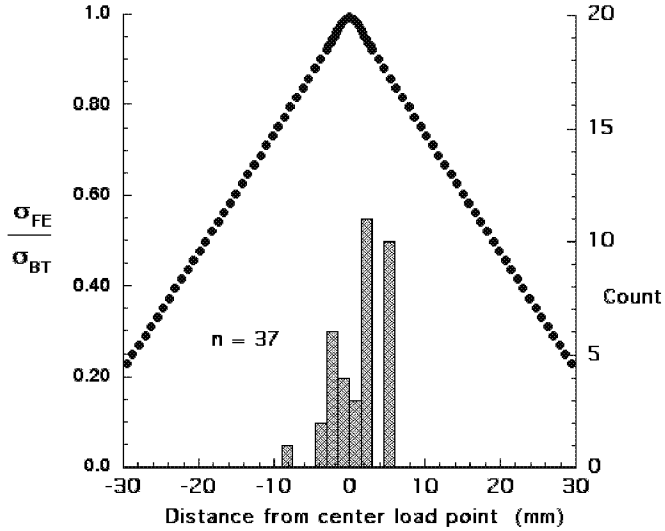

Fig.29 Comparison of Normalized Bending Stress and Failure Location 24-ply IM7/8552 3-point bending Configurations

Conf. A

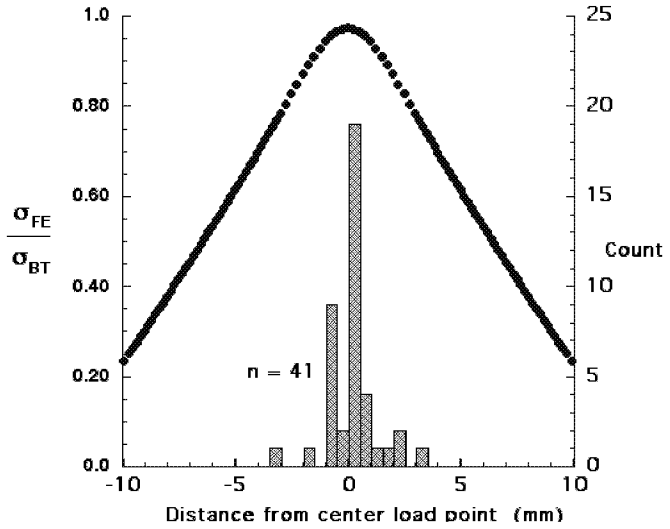

Conf. B

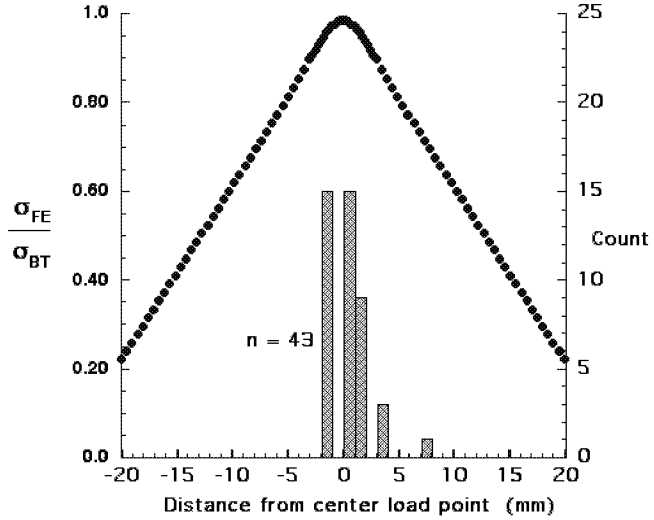

Conf. C

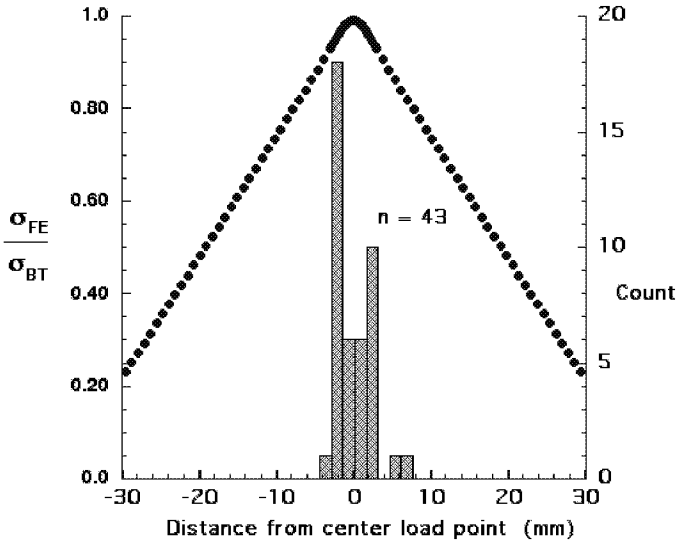

Fig.30 Comparison of Normalized Bending Stress and Failure Location 36-ply IM7/8552 3-point bending Configurations

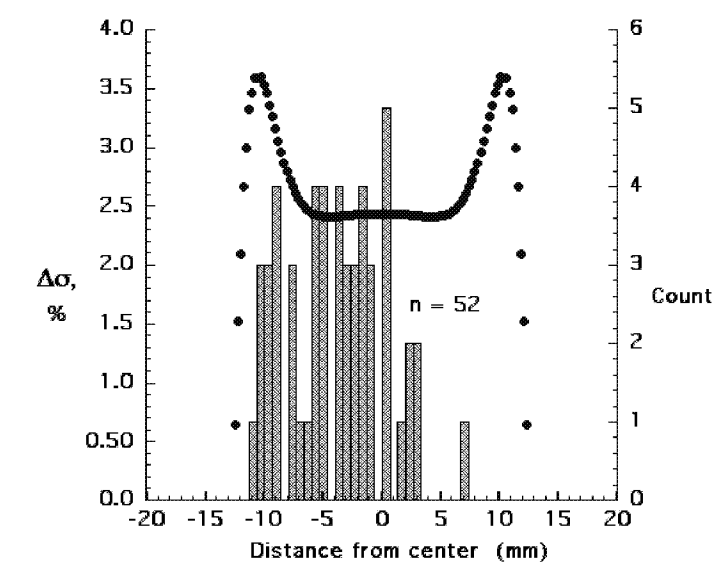

(a) Configuration A1

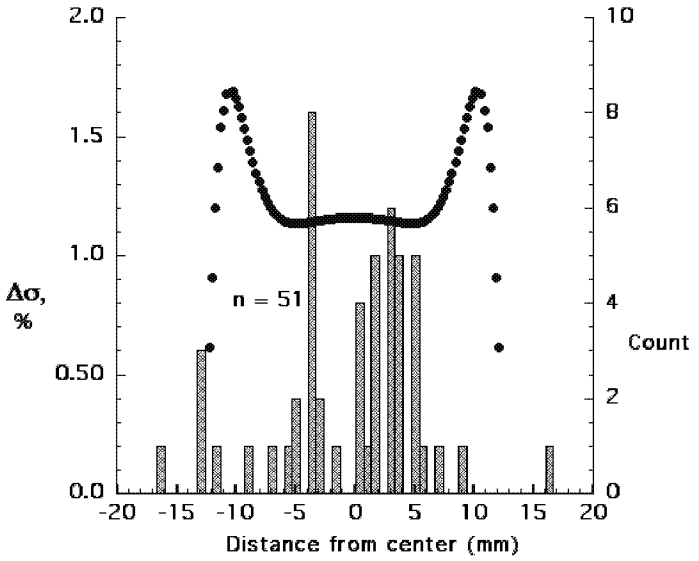

(b) Configuration A2

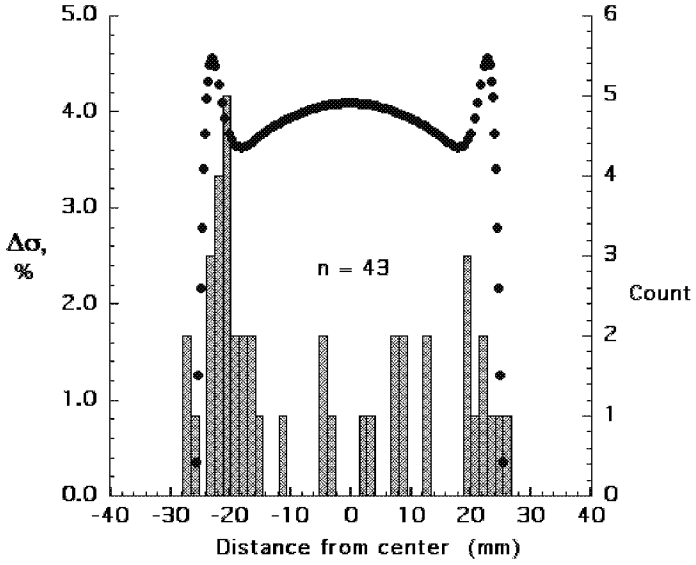

(c) Configuration B2

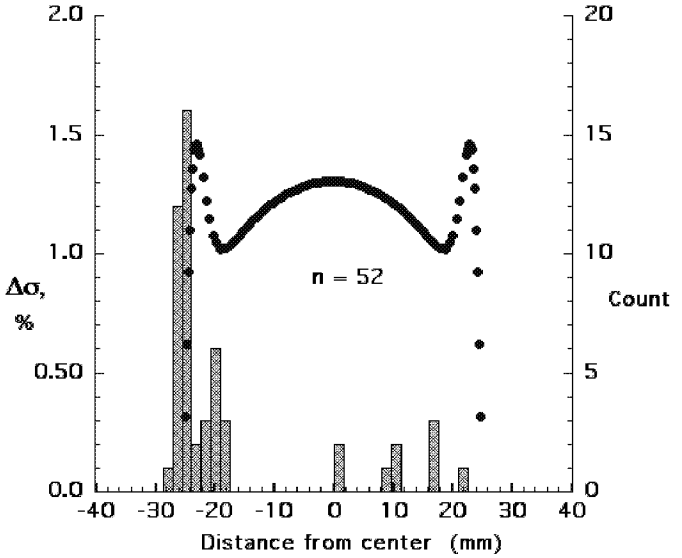

(d) Configuration B3

Fig.31 Comparison of Bending Stress Distributions and Failure Locations, S2/8552 4-point bending

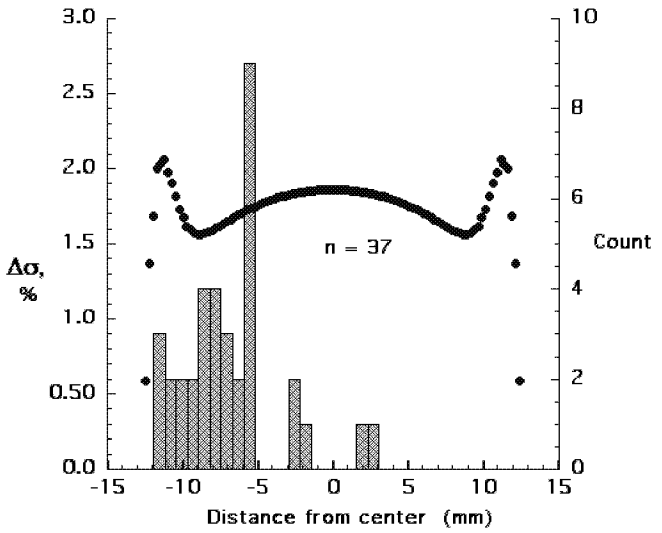

(a) Configuration A1

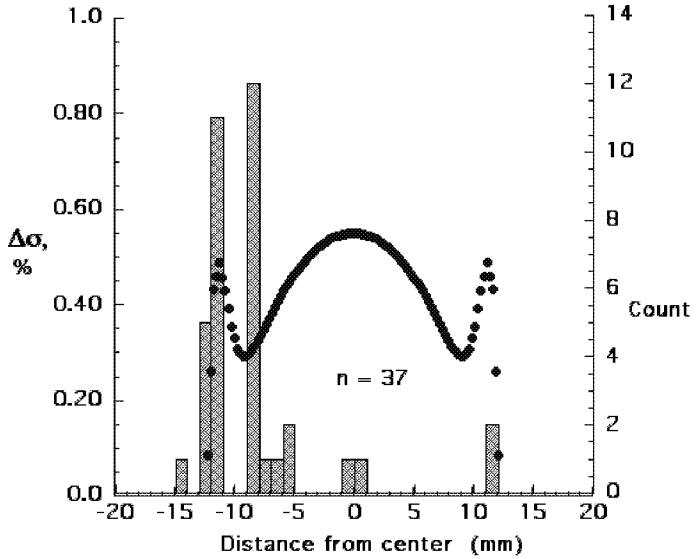

(b) Configuration A2

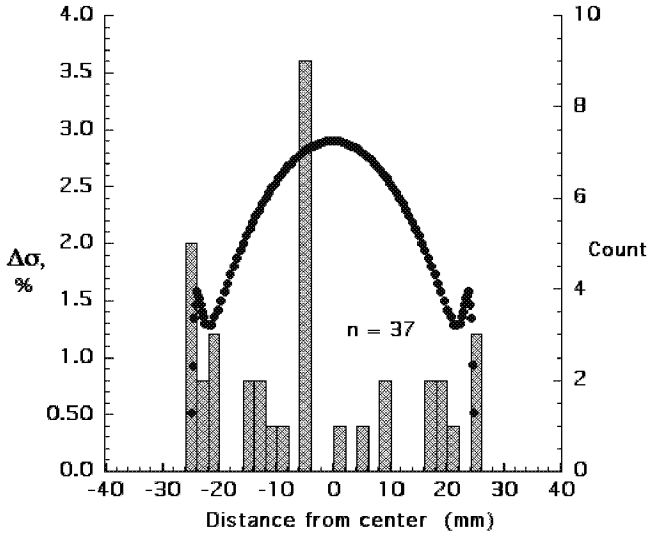

(c) Configuration B2

Not Tested

(d) Configuration B3

Fig.32 Comparison of Bending Stress Distributions and Failure Locations, 24-ply IM7/8552, 4-point bending

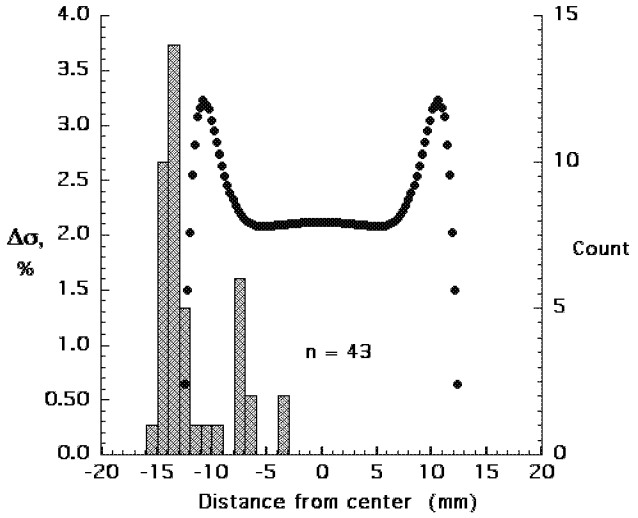

(a) Configuration A1

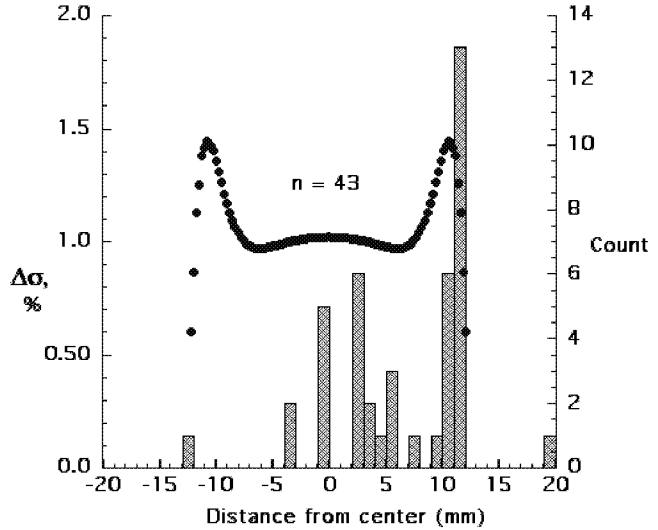

(b) Configuration A2

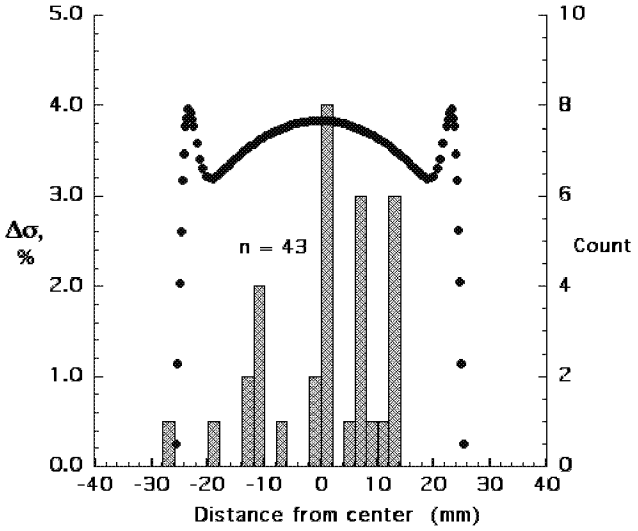

(c) Configuration B2

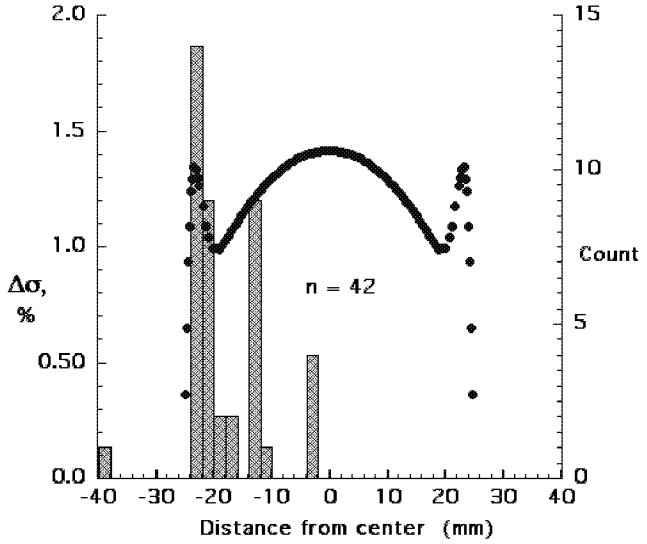

(d) Configuration B3

Fig.33 Comparison of Bending Stress Distributions and Failure Locations, 36-ply IM7/8552, 4-point bending

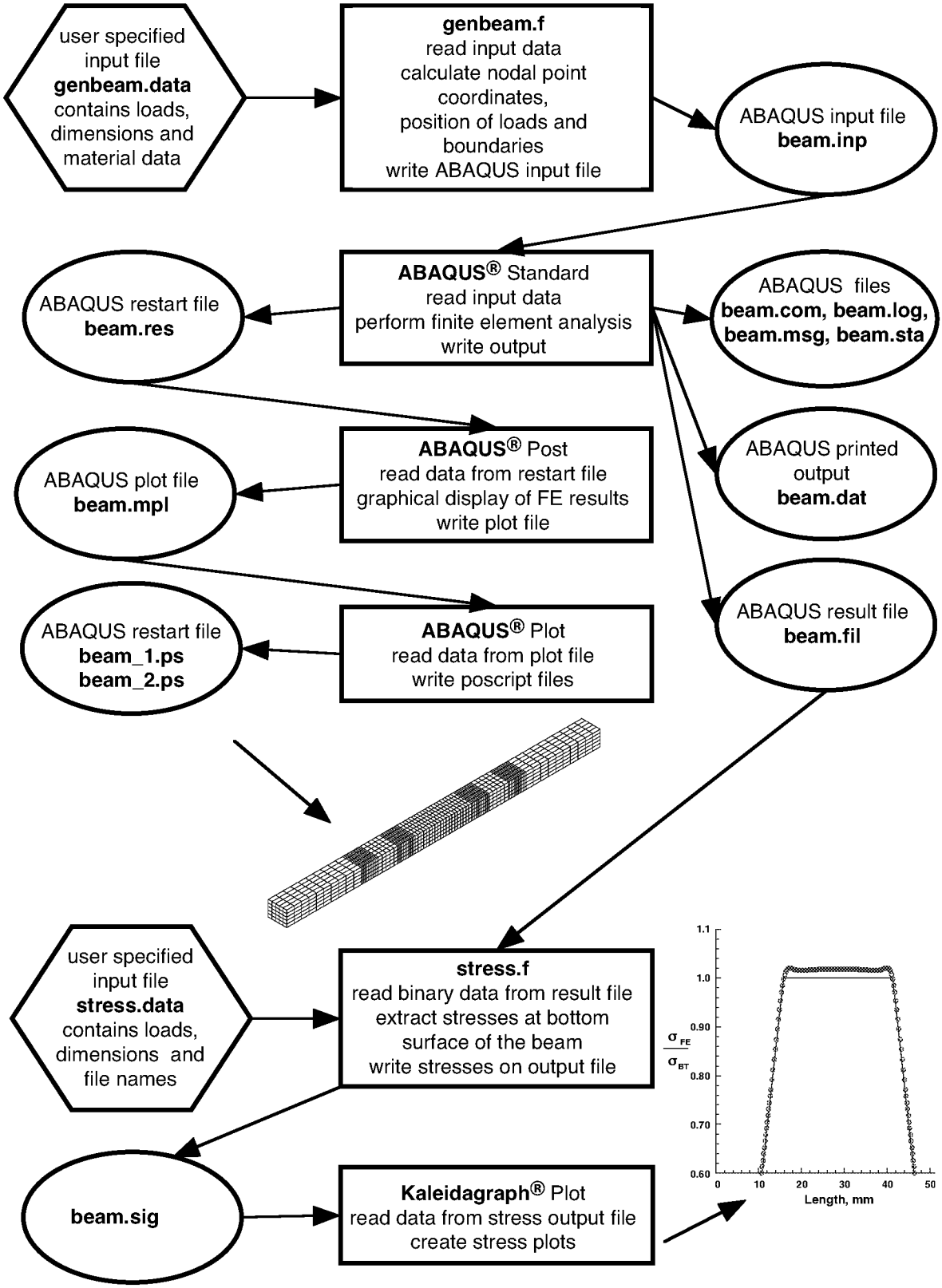

Figure A1. Flow chart of entire analysis procedure.

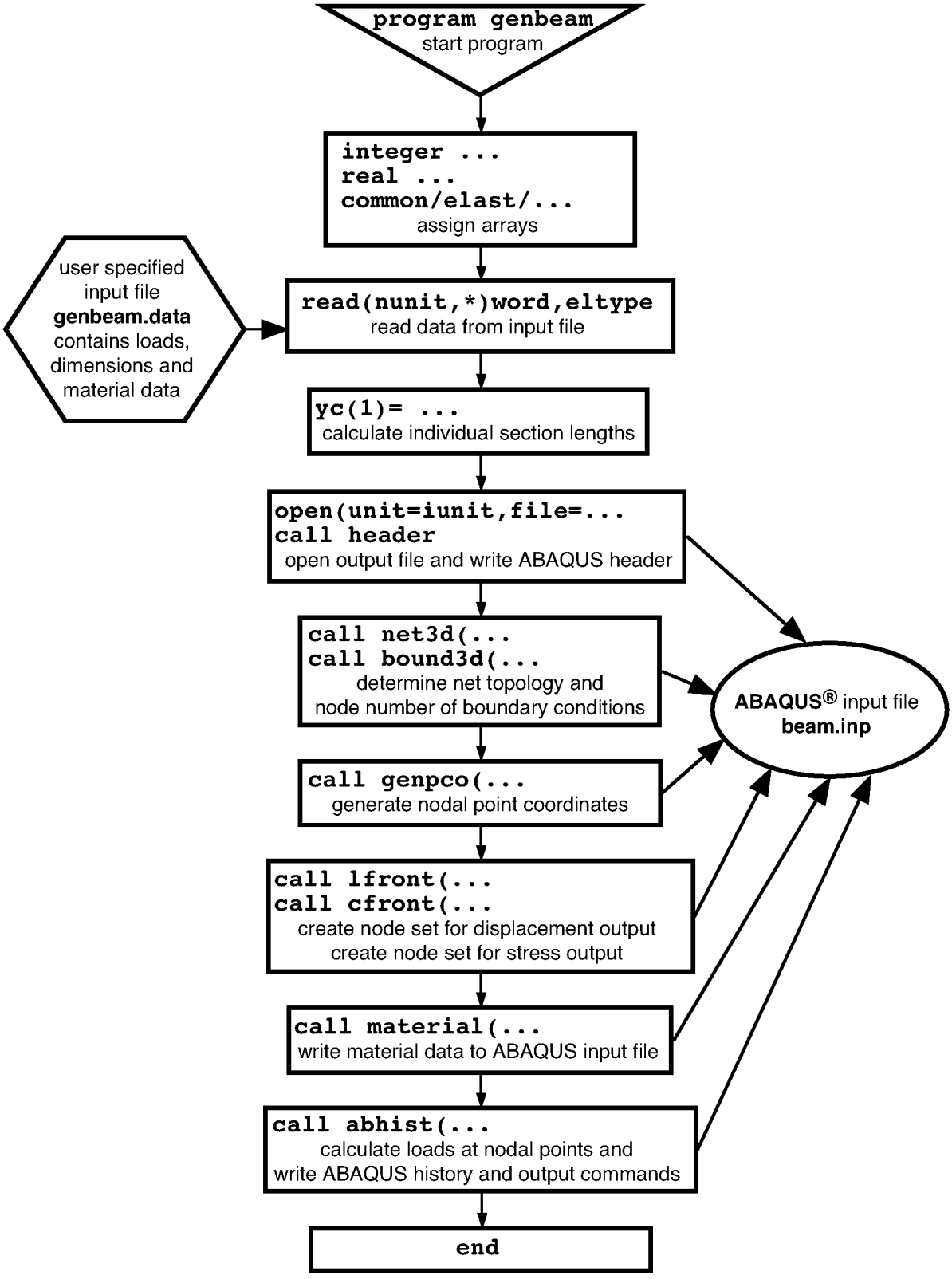

Figure A2. Flow chart of routine genbeam.f to generate finite element model.

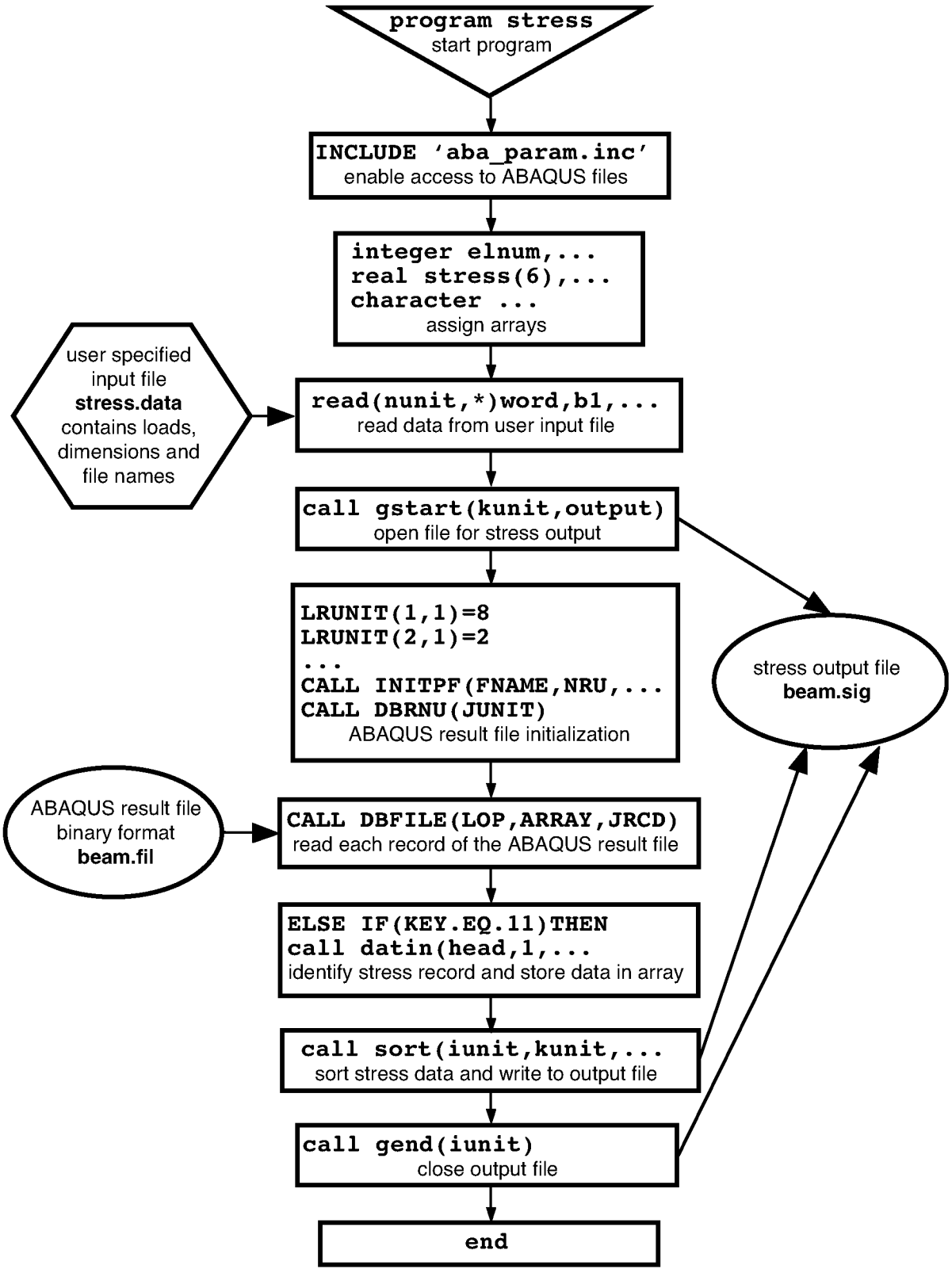

Figure A3. Flow chart of routine stress.f to retrieve stresses at the bottom of the beam.

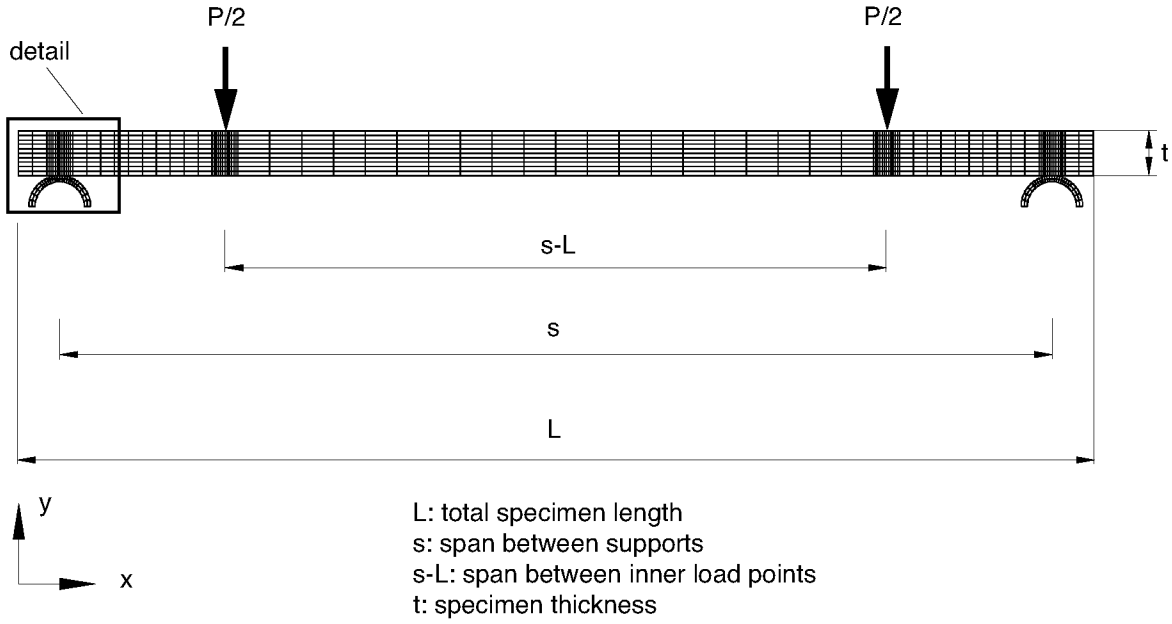

(a) Two dimensional FE model of four point bending specimen with modeled rollers

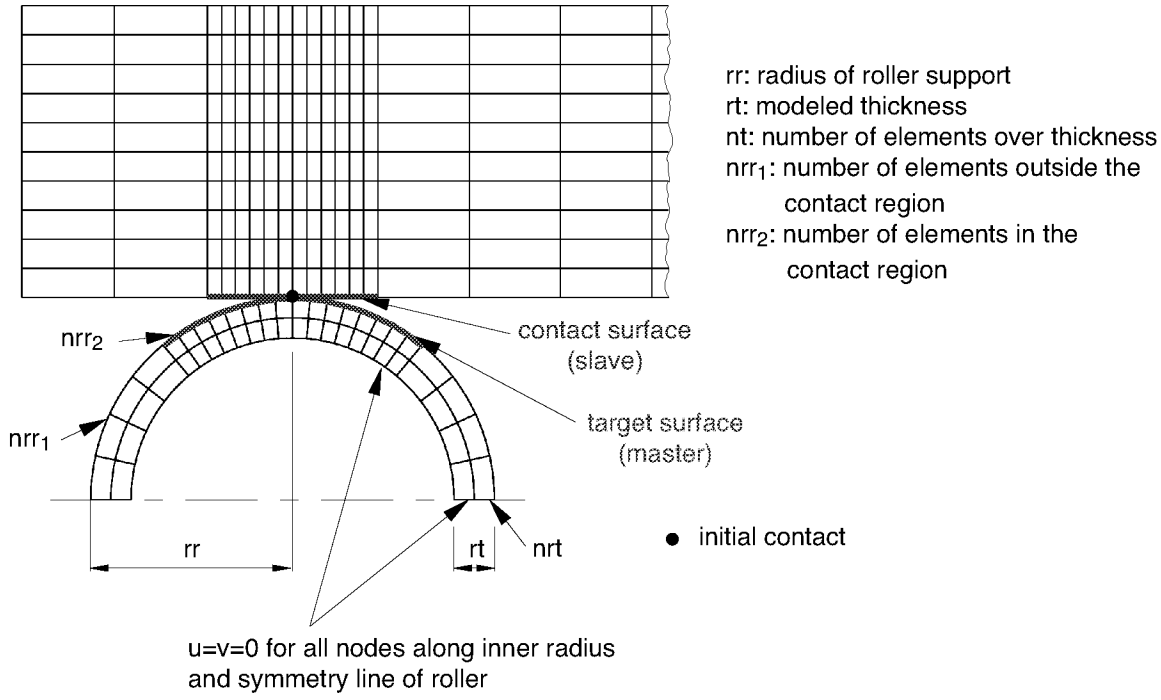

(b) Detail of modeled roller and contacting surfaces

Figure A4. FE model with rollers and corresponding load and boundary conditions

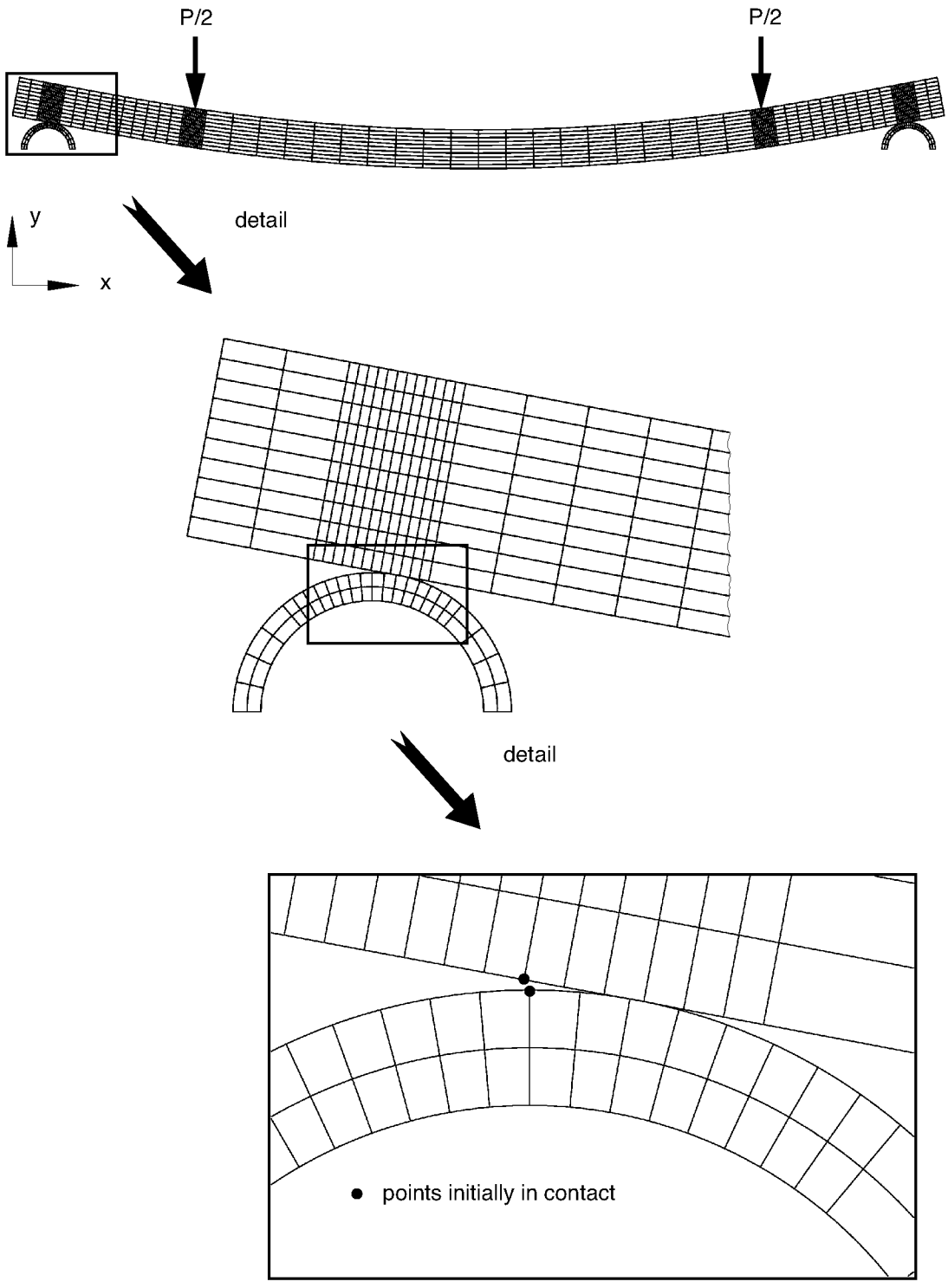

Figure A5. Deformed FE model with details of modeled rollers and contacting surfaces

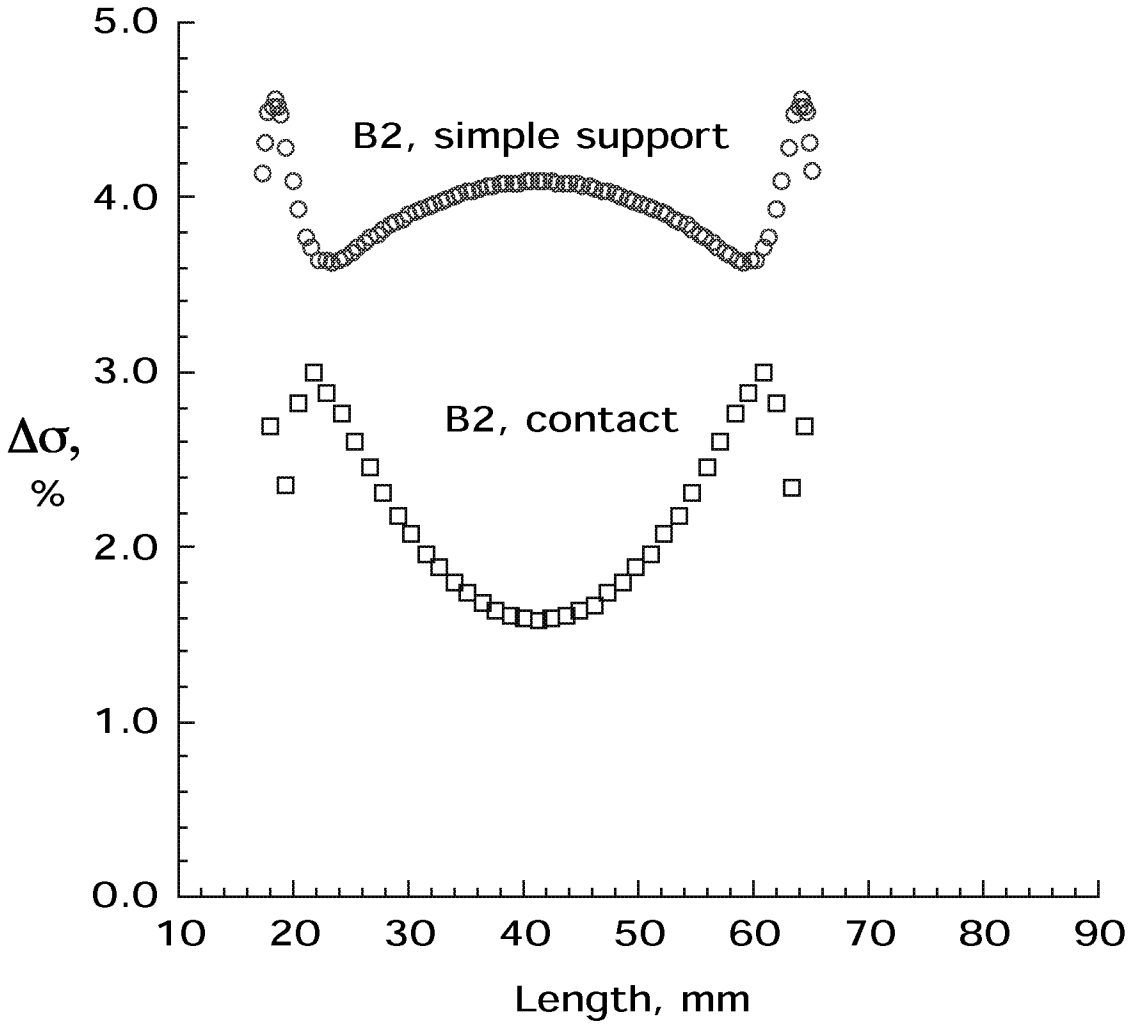

Fig. A6a Comparison of Discrepancy between Beam Theory and 2D Plane-Stress non-linear FE analysis, S2/8552 4-Point Bend Configuration B2

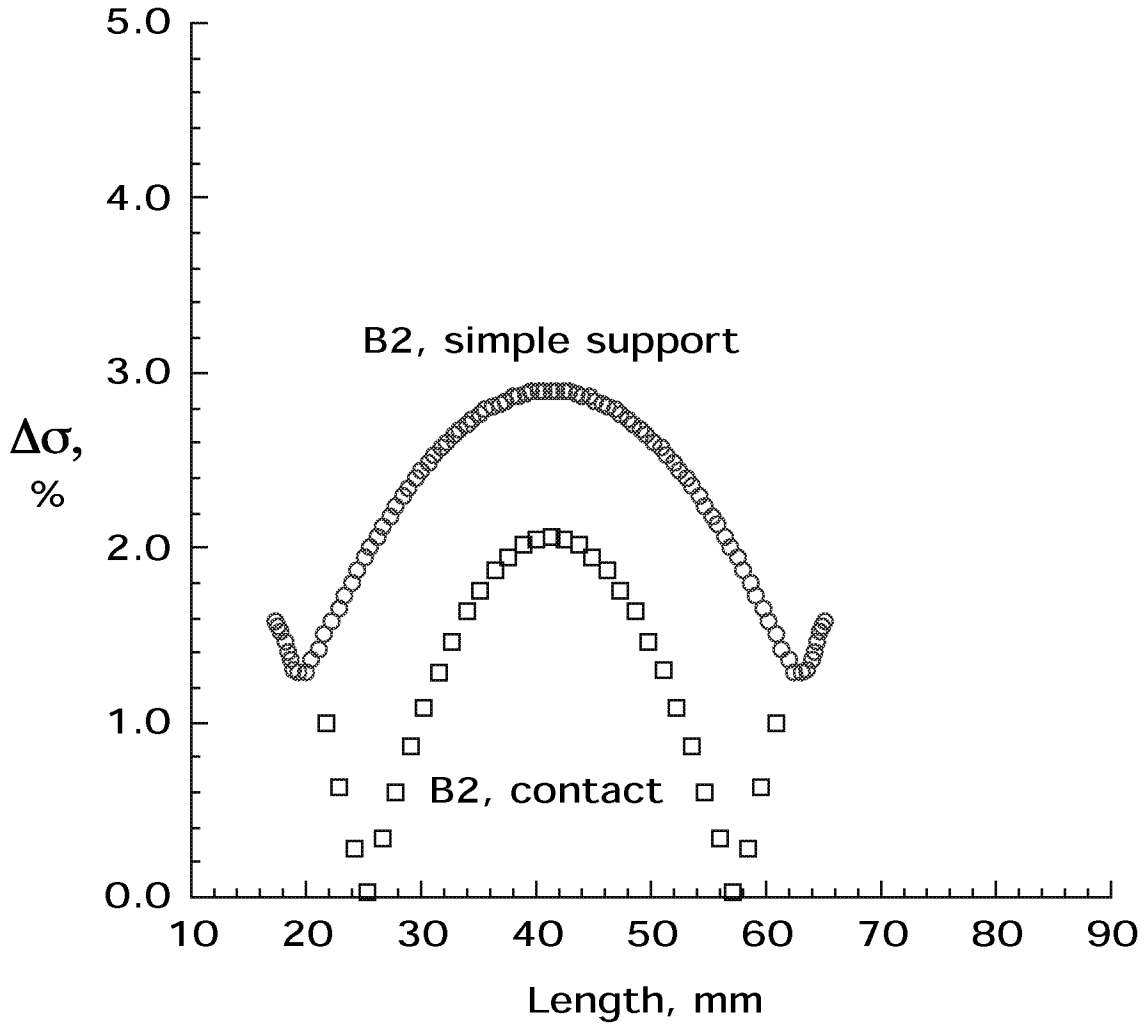

Fig. A6b Comparison of Discrepancy between Beam Theory and 2D Plane-Stress non-linear FE analysis, 24-ply IM7/8552 4-Point Bend Config. B2

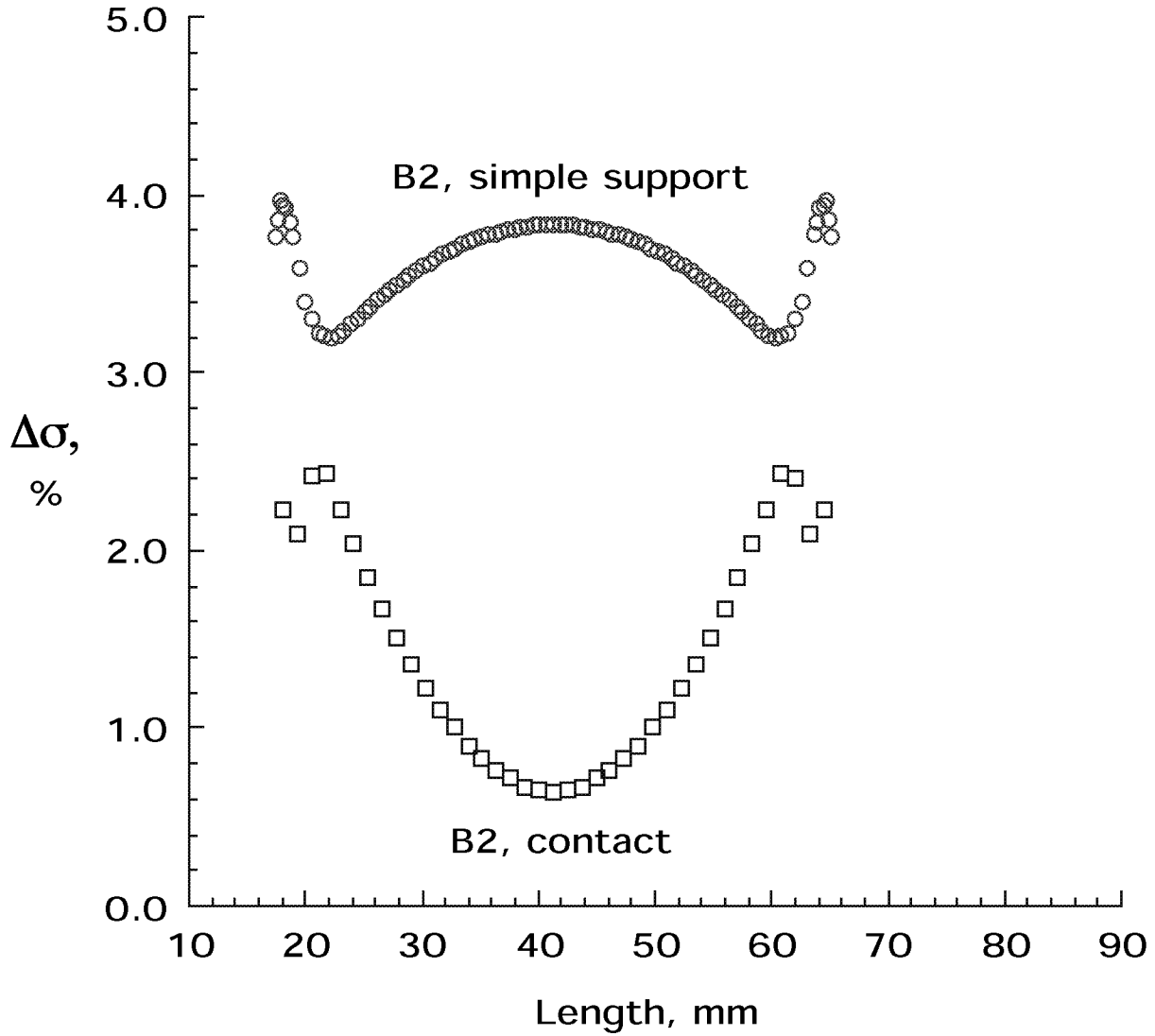

Fig. A6c Comparison of Discrepancy between Beam Theory and 2D Plane-Stress non-linear FE analysis, 36-ply IM7/8552 4-Point Bend Config. B2

REPORT DOCUMENTATION PAGE

Form Approved
OMB No. 0704-0188

1. AGENCY USE ONLY (*Leave blank*)	2. REPORT DATE	3. REPORT TYPE AND DATES COVERED
	October 2001	Technical Memorandum

4. TITLE AND SUBTITLE
Analysis of Ninety Degree Flexure Tests for Characterization of Composite Transverse Tensile Strength

5. FUNDING NUMBERS
WU 581-10-21-01

6. AUTHOR(S)
T. Kevin O'Brien, Ronald Krueger

7. PERFORMING ORGANIZATION NAME(S) AND ADDRESS(ES)
NASA Langley Research Center
Hampton, VA 23681-2199

U.S. Army Research Laboratory
Vehicle Technology Directorate
NASA Langley Research Center
Hampton, VA 23681-2199

8. PERFORMING ORGANIZATION REPORT NUMBER
L-18114

9. SPONSORING/MONITORING AGENCY NAME(S) AND ADDRESS(ES)
National Aeronautics and Space Administration
Washington, DC 20546-0001
and
U.S. Army Research Laboratory
Adelphi, MD 20783-1145

10. SPONSORING/MONITORING AGENCY REPORT NUMBER
NASA/TM-2001-211227
ARL-TR-2568

11. SUPPLEMENTARY NOTES
Krueger: ICASE, NASA Langley Research Center, MS 132 C, Hampton, VA 23681-2199

12a. DISTRIBUTION/AVAILABILITY STATEMENT
Unclassified-Unlimited
Subject Category 24 Distribution: Nonstandard
Availability: NASA CASI (301) 621-0390

12b. DISTRIBUTION CODE

13. ABSTRACT (*Maximum 200 words*)

Finite element (FE) analysis was performed on 3-point and 4-point bending test configurations of ninety degree oriented glass-epoxy and graphite-epoxy composite beams to identify deviations from beam theory predictions. Both linear and geometric non-linear analyses were performed using the ABAQUS® finite element code. The 3-point and 4-point bending specimens were first modeled with two-dimensional elements. Three-dimensional finite element models were then performed for selected 4-point bending configurations to study the stress distribution across the width of the specimens and compare the results to the stresses computed from two-dimensional plane strain and plane stress analyses and the stresses from beam theory. Stresses for all configurations were analyzed at load levels corresponding to the measured transverse tensile strength of the material.

14. SUBJECT TERMS
Transverse Tensile Strength, matrix cracking, finite element analysis,

15. NUMBER OF PAGES
58

16. PRICE CODE
A04

17. SECURITY CLASSIFICATION OF REPORT	18. SECURITY CLASSIFICATION OF THIS PAGE	19. SECURITY CLASSIFICATION OF ABSTRACT	20. LIMITATION OF ABSTRACT
Unclassified	Unclassified	Unclassified	UL